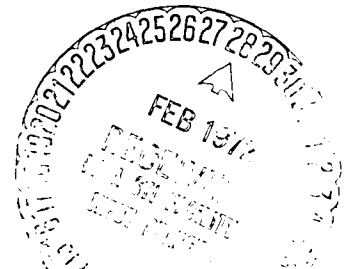
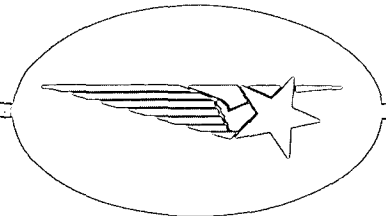


148



Lockheed

Reproduced by
NATIONAL ARCHIVAL
INFORMATION SERVICE
U.S. Department of Commerce
Springfield VA 22151

PALO ALTO RESEARCH LABORATORY

LOCKHEED MISSILES & SPACE COMPANY • A GROUP DIVISION OF LOCKHEED AIRCRAFT CORPORATION

PALO ALTO, CALIFORNIA

22
(NASA-CR-125607) SPATIAL AND SPECTRAL
STUDIES OF SOLAR PHENOMENA Final Report,
Sep. 1970 - Aug. 1971 K.L. Harvey, et al
(Lockheed Missiles and Space Co.) Sep.
1971 49 p

N72-18792
Unclas
CSCL 03B G3/29 17341

FINAL REPORT

SPATIAL AND SPECTRAL STUDIES
OF SOLAR PHENOMENA

LMSC D24368

September 1971

Lockheed Solar Observatory

Contributions by:

Karen L. Harvey

John L. Kulander

Sara F. Martin

Harry E. Ramsey

Submitted to the National Aeronautics and Space Administration
upon completion of Contract NASw 2160

LOCKHEED MISSILES & SPACE COMPANY

INTRODUCTION

The work completed under contract covered a wide range of research activities including instrument assembly and testing, acquisition of observations, analysis of data, and theoretical studies. Throughout the period of the contract, September 1970 through August 1971, work proceeded simultaneously in four different areas of solar research. These were: (1) assembly and testing of the previously designed and fabricated components of a multiple-slit H α spectrograph, (2) simultaneous observations of the wings of the H α line with a newly modified filter, (3) analysis of H α high resolution observations in conjunction with magnetic field observations obtained at Kitt Peak, and (4) theoretical analysis of the D₃ line of HeI. The results achieved in each of these areas are described in the following sections of this report by the individuals primarily responsible for each task.

SECTION I
THE MONOCHROMATIC MULTIPLE-SLIT SPECTROGRAPH

Prior to this contract, a unique spectrograph was designed at Lockheed for obtaining multiple spectra on a chosen line in the visible spectrum. The components of the spectrograph were provided by Lockheed. Under this contract, the testing, final assembly, and initial observations were made.

As could be expected for any new observational system, the initial design was slightly altered, and minor changes had to be made in some components. A field lens was incorporated at the location of the multiple slit assembly to eliminate vignetting of the final image. The grating holder was modified to accommodate the oversized grating which was received. More adjustable lens holder mounts were added in order to test different combinations of lenses.

The concept of a multiple-slit spectrograph depends on using a filter to isolate the spectrum line for which multiple, parallel spectra are to be taken. The spectrograph was tested with both 10 Å and 5 Å H α interference filters. It was decided that the 5 Å H α filter would be best for initial observation since it would permit using twice as many slits as to 10 Å filter for the limited region of the sun to be photographed. The 5 Å filter was mounted in thermally controlled oven for wavelength stability.

The experimental multiple-slit assemblies were produced by evaporating an aluminum coating onto lenses placed behind stretched parallel wires. Tests of the sharpness of the slit edges showed them to be more than adequate for the initial low dispersion observation. It was empirically determined that 0.001 inch slits separated by 0.050 inch yield good resolution, adequately short exposures, and appropriate spacing for the prefilter having a half-width of 5 Å.

A narrow band H α filter was required for the "slit-jaw" images in order to allow the observer and analyst to identify the slit locations on an H α image. A 1/2 Å bandpass Halle' filter was loaned to Lockheed by NOAA for a minimum period of one year in exchange for Lockheed Observatory's replacement of one broken and two defective elements. The filter was successfully repaired and now delivers an excellent H α image when used in a good optical system under optimum atmospheric image quality.

This NOAA filter and the Lockheed 5324 Å filter were both used in the final visual test on the quality of 10" objective, field lens and imaging lens which feed the spectrograph. This combination of optics yielded visual images resolving structure smaller than one arc second. This is better than any system yet tested at Lockheed Observatory. It is expected that improved high resolution films will be forthcoming during periods when the atmospheric image quality is consistently good.

The other components which tested satisfactorily are the polarizing beam-splitter, a pair of negative lenses, the Littrow lens and grating. In addition, the transfer optics which relay the "slit jaw" image to the same film plane as the spectral images seem satisfactory. However, due to scattered light from the coelestat delivering the solar image and also questionable "seeing" conditions in the optics tunnel where the components were tested, the final verification of the quality of these components awaits the mounting and operation of the complete system in the solar spar.

This program is being continued under contract with NOAA by means of NASA support. It is anticipated that time-lapse solar photography obtained with the above described system will yield new data for analysis on the flash phase of solar flares, changes in filaments and prominences, and rapidly changing flare-associated phenomena which are rarely observed using conventional spectrographs.

SECTION 2
NARROW-BAND H α DOPPLER STUDIES

2.1 Observations

The objective has been narrow-band H α Doppler studies of the highest obtainable resolution from simultaneous observations in both wings of the H α line. In order to acquire these data it was necessary to modify a birefringent filter.

By April 1971 the fabrication of the two-peak, 0.3A filter was completed. It was installed on the NASA solar span in the 7 inch aperture refractor with a new two-frame 35 mm camera incorporating a polarizing beam-splitter. The filter has the profile shown in Figure 2.1 with two 0.3A peaks separated by 0.6A. The polarizing beam-splitter of the two-frame camera separates the transmission peaks into two images displaced along the length of the film. Special effort was made to give the images precise single frame separation relative to the film perforations. This will permit exact super-position of images in cini-projection, color combination and photo-subtraction.

During the period April 1971 through August 1971 we obtained eleven thousand feet of 35 mm time-lapse studies with simultaneous picture pairs at 15 second intervals. The system was steadily improved, especially in filter performance and frame registration. We were fortunate during the period to record three disk passages of the largest active region in the southern hemisphere of this solar maximum. We are presently recording the fourth passage of this region as part of a special cooperative study with Kitt Peak National Observatory.

Two 16 mm copies, black and white, have been made of the eleven thousand feet of 35 mm negative. One full copy is retained at Lockheed for study

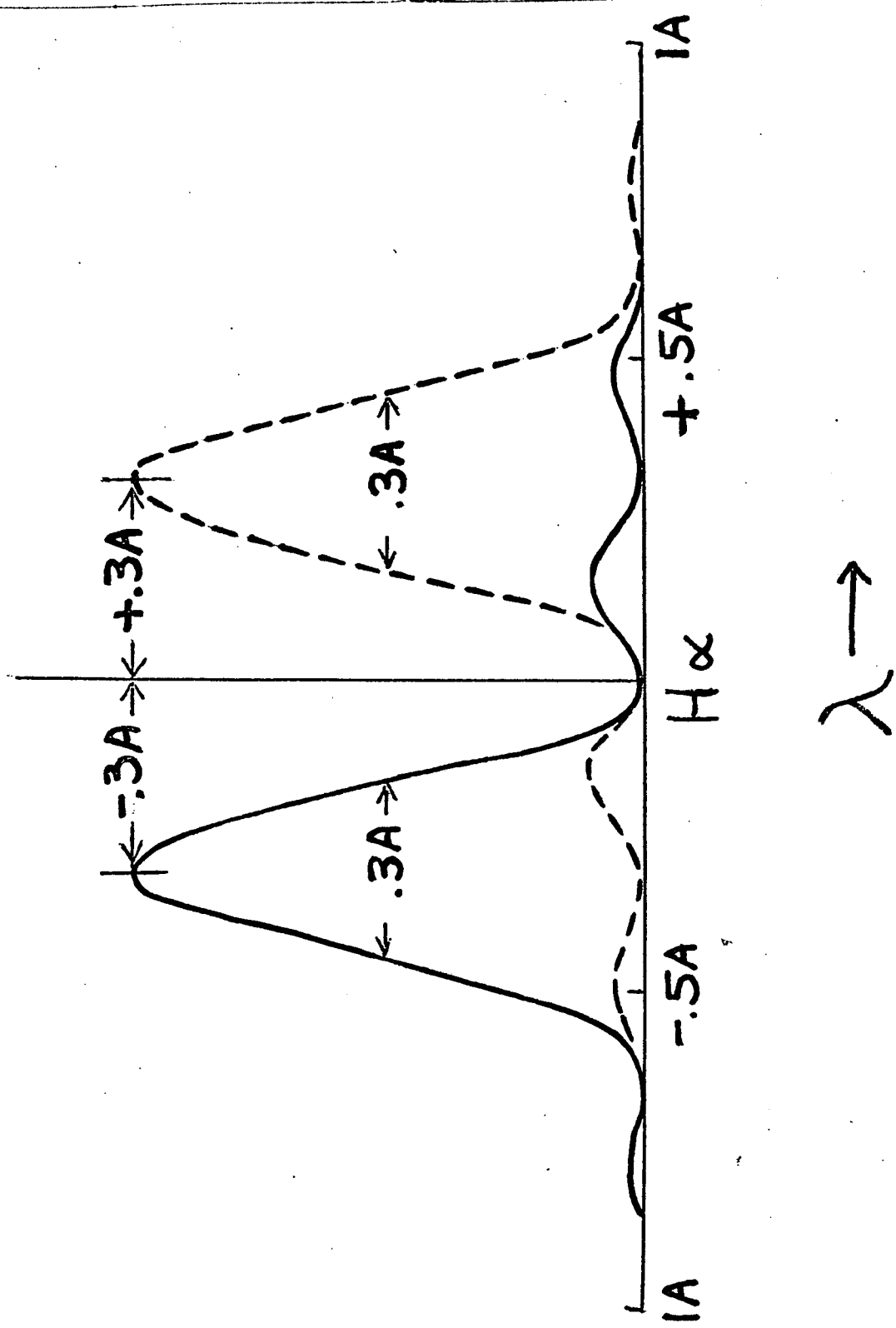


Figure 2.1. Transmission profiles of the two-peak H α filter for Doppler velocity studies

and one full copy has been delivered to Dr. Constance Sawyer at NOAA for separate study.

2.2 Experiments in Color Combinations

Color combinations of several days involving interesting activity have been made on the optical printer at Lockheed to assess the value of color cine-projection versus black and white flicker movies. The color films thus far studied appear to have vastly improved capability for detection and interpretation of transient and subtle events. Activity and relationships readily seen in color in some instances can not be found in black and white projection. We tried to obtain superposition in color with maximum spatial resolution, but this has not been yet fully realized. There is no technical reason for not routinely achieving this in the near future.

By separating our Doppler pairs along the length of the film, we have the option of 16 mm color combinations at the same material cost as for 16 mm black and white. When two frames are combined in color, the footage is one half that of a black and white copy. The cost of 16 mm color print stock is less than twice the cost of black and white. Thus raw color stock costs slightly less than black and white stock.

The precise separation of picture pairs along the length of our film also offers the option of convenient photographic subtraction of entire time-lapse runs. After making a gamma 1.0 contact print of the original, the two films are displaced one frame and bi-packed in the optical printer. The super-imposed simultaneous frames are then exposed on copy film by an automatic skip-frame operation.

The movie-photo-subtraction has not been done because the Lockheed optical printer will require an improvement to permit the film bi-pack operation. This improvement is planned in the near future, and the first use of the photo-subtraction will be the study of five minute oscillations of the quiet chromosphere.

2.3 Solar Flares and Transient Emission

To date we have studied 120 small flares observed on the solar disk with the two-peak 0.3 Å filter. We tried to center the 0.3 Å filter peaks at H α -0.3 Å and H α +0.3 Å (Figure 2.1) but minor filter temperature excursions frequently decentered the filter by plus or minus 0.1 Å.

Statistically, we must presently conclude that emission centers of the small flares seen on the disk are essentially identical at all times in their life when observed at +0.3 Å and -0.3 Å. The first 80 flares observed were consistently slightly brighter and larger in the red wing, but it now appears that this effect was, at least partially, a filter weakness. For the 40 flares observed following a filter adjustment, the red and blue wings appear exactly identical at all times (Figure 2.2).

We observed only one really energetic major flare, an Importance One bright, occurring in the period when the red-wing filter contrast was higher. In spite of this filter effect, the red wing dominance observed in the pre-maximum phase (Figure 2.3) is probably real. This flare compares closely with the flares observed in our broad-band H α Doppler studies at H α + and -1.2Å (Lockheed 1968). The red wing flare precedes the blue wing in size and intensity by about 30 seconds in time at flare start, with the two becoming about equal at flare maximum. The slight red dominance observed here after maximum is probably instrumental.

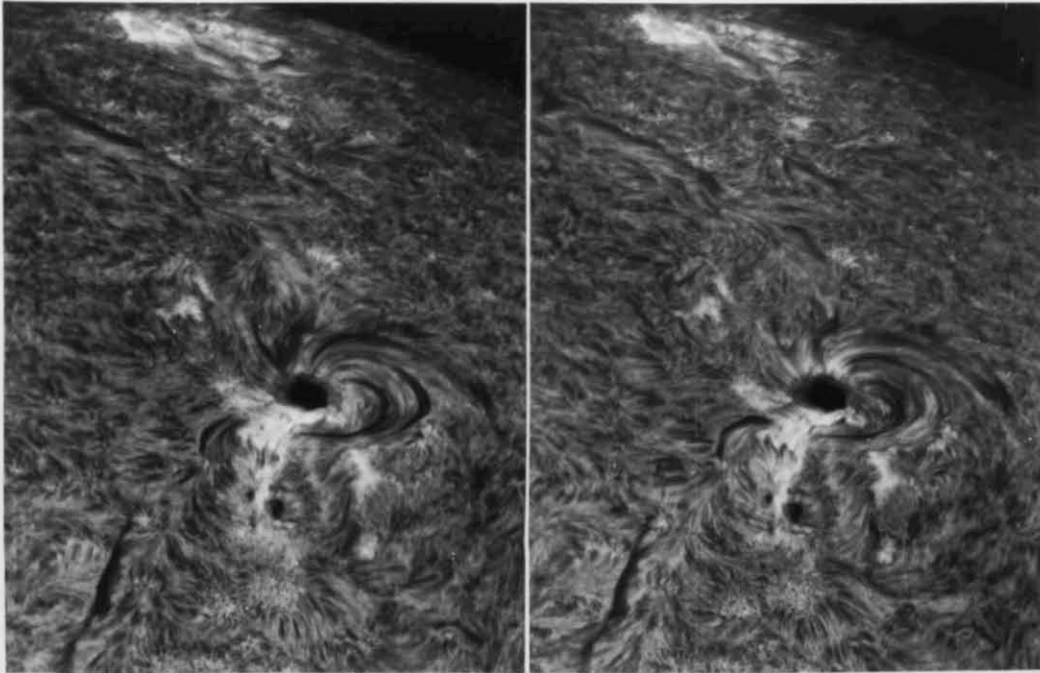
Admittedly, the "red flash" (Ellison 1949) is short-lived and less pronounced in our narrow-band Doppler studies with small displacements from line center. Nevertheless its observance is significant to Hyder's (1969) in-flow impact model.

In the few cases where distinct Doppler differences in flare emission were observed, we usually found a reciprocal dark absorption feature in the opposite wing.

A single observation of a typical flare-surge near the limb (Figure 2.4), associated with downflow from a quasi-eruptive prominence, is judged worthy of description. The Doppler differences in flare emission were very fast changing and subtle but of distinct character. In the early stages the blue

24 JULY 71

1 X 10⁵ KM

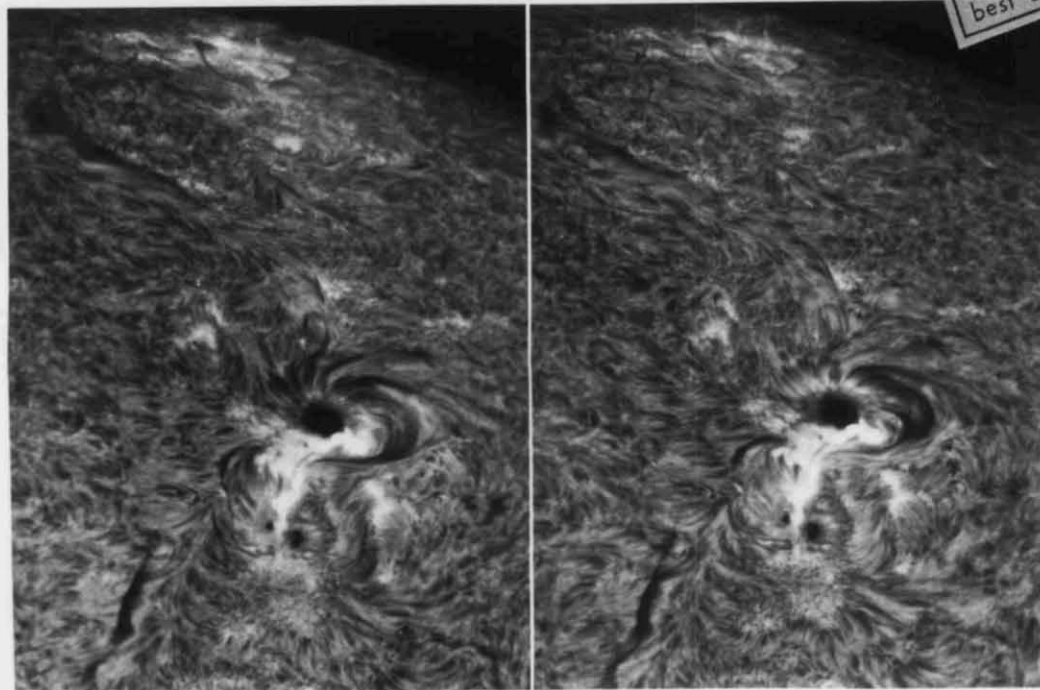


H α -0.3Å

1658:00

H α +0.3Å

Reproduced from
best available copy.



1756:00

Figure 2.2. The small flare near the spot shows no Doppler difference, while nearby filament and fibrils show strong differences suggesting a giant vortex.

1 JULY 71

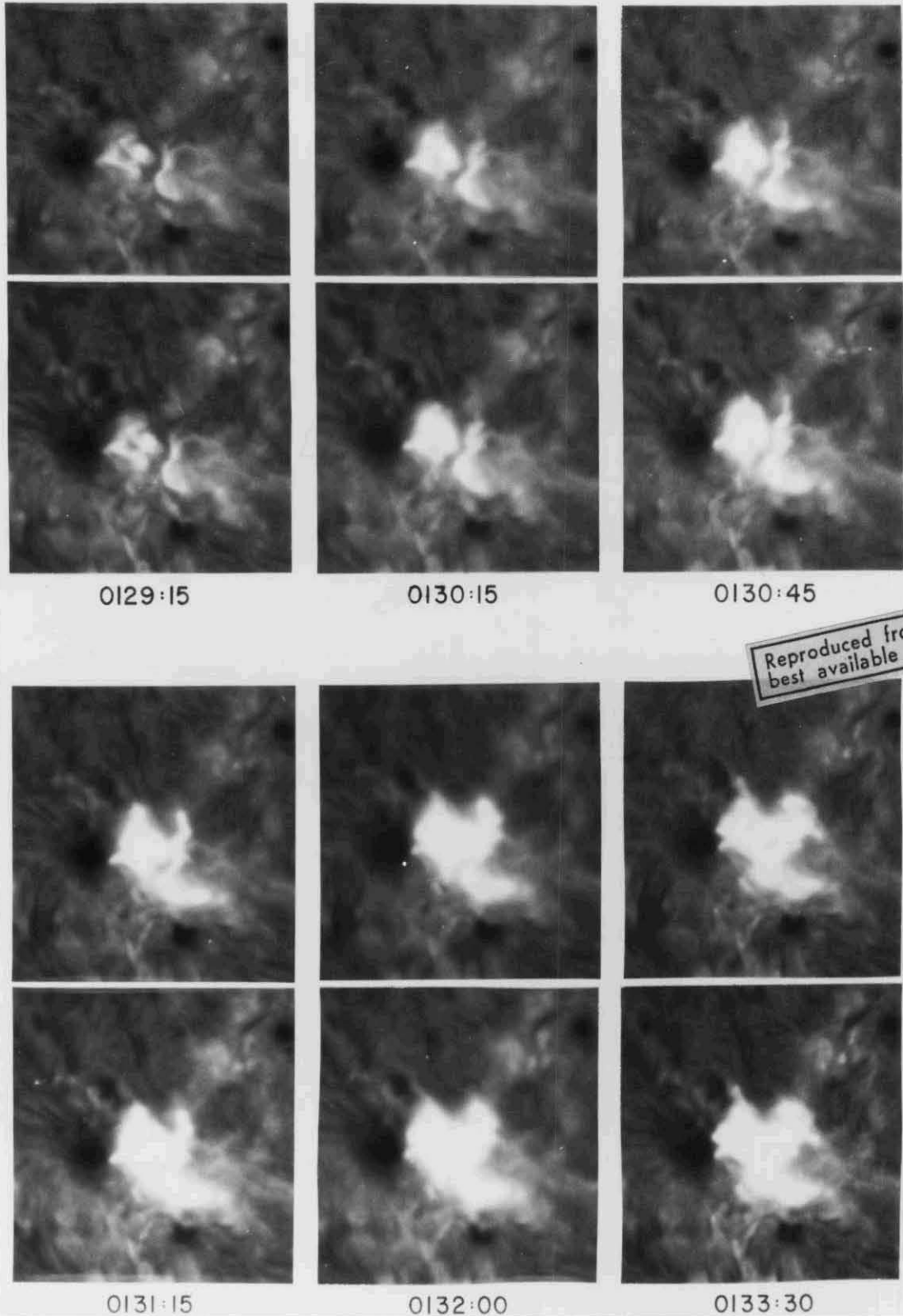
— 1×10^5 KM —

Figure 2.3 At flare start, the red wing, greater in area and intensity, precedes the blue wing by about 30 seconds. The two wings become nearly equivalent at flare maximum.

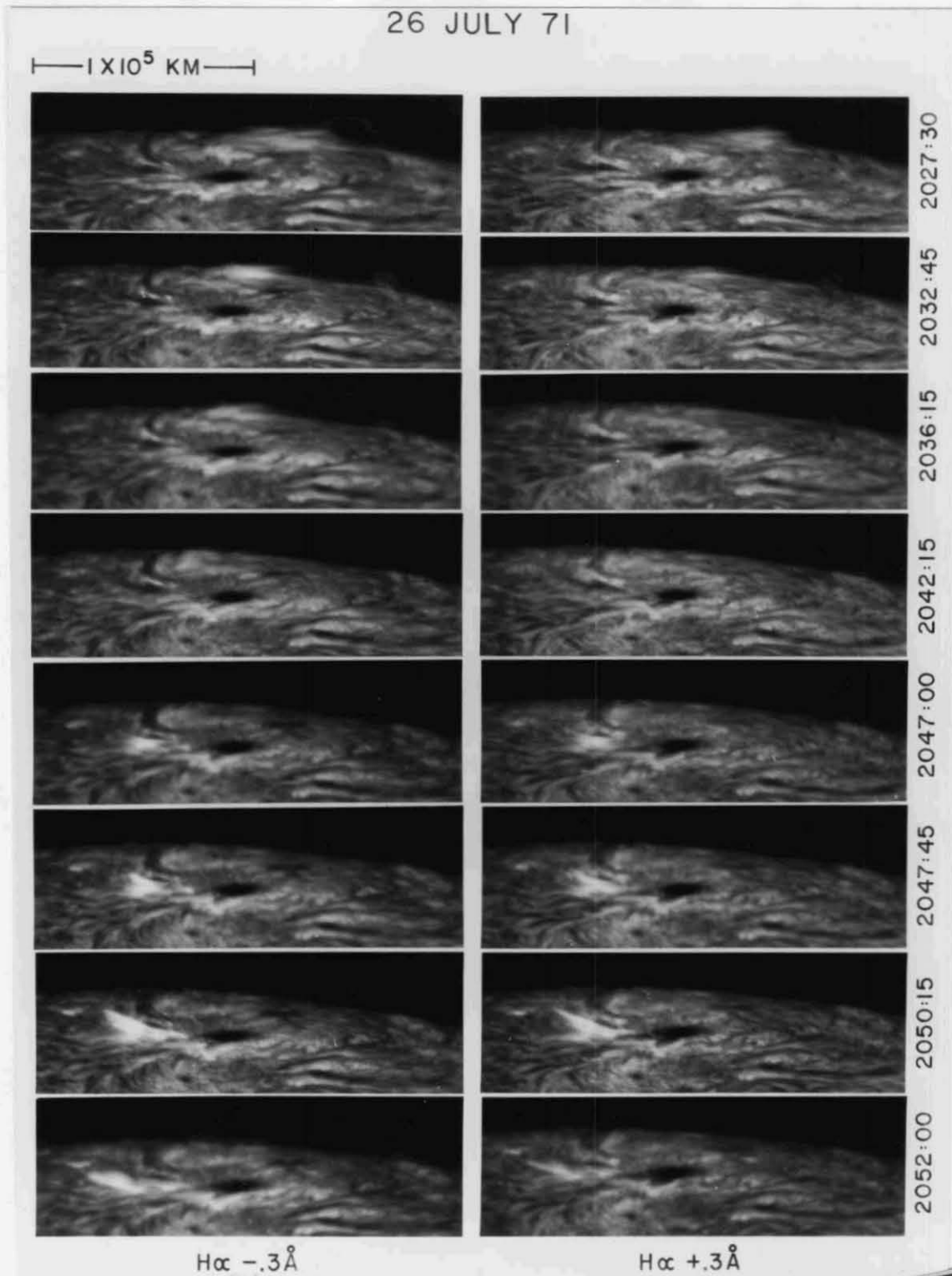


Figure 2.4. An emission feature moving from a quasi-eruptive prominence appears to descend along an existing filament and thence associates with a small flare-surge.

wing is brighter, more compact, and the red wing less bright, longer and more extensive. The action resembles a much accelerated arch filament or loop prominence condensation, with one end lifted and blowing outward while the other flows down. This flow, in opposite directions in a typical flare-surge, makes its dynamics more analogous to observations of other ordinary flares.

Evidence for small flares associated with downflow is best displayed in the flare associated events observed with the new filter system. In several instances a "moving emission" feature displaying appropriate Doppler differences appeared to be directly associated with a small flare upon impacting the chromosphere. In the case of the previously described flare-surge (Figure 2.4), these emission features come from a quasi-eruptive prominence and appear to descend along an existing filament to associate with the small flare-surge. In many cases the moving emission appears to originate in another part of an active region, travels along a small filament and coincides with a small flare upon arrival at a new location. Frequently, the source of the moving emission displayed a rapid short-lived brightening at the onset, followed by rapid changes in the connecting filament. Measured velocities of moving emission along filaments ranged from 50 to 120 km/sec.

The flare-associated activity so far observed with the new system, especially in the films in which the Doppler pairs are color combined, suggests intimate connection between separate centers in active regions, and between widely separated regions, with evidence that some solar flares are associated with observed downflow.

2.4 New Region Activity

All young regions observed were characterized by pronounced "downflow" at the ends of the arch filament systems (Bruzek 1967). The downflow at the ends of the arch filaments is much more significant than the upward motion at their centers. The upward motion was barely discernable in our observations.

The pronounced downflow associated directly with the emission and transient brightenings produces a dominance of emission in the blue wing for new regions at center disk. In most cases observed, the blue-sided emission was

exactly co-spatial with the dark ends of the arch filaments in the red wing. Again we have chromospheric emission associated with downflow (Hyder 1967).

Our observations are consistent with Weart's (1970) picture of emerging magnetic flux and further emphasize the importance of "condensation and downflow" in the growth process of plage and sunspot.

2.5 Observations of H α "Evershed" Effect

The most frequent and obvious Doppler differences observed with this filter configuration is the (Evershed 1948) flow into sunspots. The limb is represented by darkening of fibril and filament structures on the limb side of sunspots observed in the blue wing (Figures 2.2 and 2.5). The effect is reversed at the center of the disk (Figure 2.5) with filament and fibril structures darker in the red wing. Also, striae in sunspot penumbrae appear distinctly darker in the red wing at center disk. The flow towards the sunspots is strongly transverse and the Doppler differences are best observed at radius vectors of 0.8 or more on the limb side of spots. The degree of Evershed flow observed in H α presently appears strongest with active growing sunspots.

Along with the darkening of fibrils and filaments, there is a reciprocal brightening in the opposite wing generally in the form of a bright ring around the penumbral border.

2.6 Observing Rotation of the H α Chromosphere

As we observe with the two-peak, 0.3 Å H α filter it is necessary to balance the filter centering for each new location on the solar disk in order to remove the observed effects of solar rotation. Rotation of the chromosphere is seen as a change in background structure dominated by an overall increase or decrease in photospheric light (Figure 2.6). The experienced observer can easily see the structural differences from limb to limb. However, the overall intensity change represents a more readily measured quantity to roughly measure the sensitivity of the filter to Doppler velocity change. We measured the integrated photographic density of picture pairs at selected places of undisturbed chromosphere using a field aperture of one minute of arc diameter.

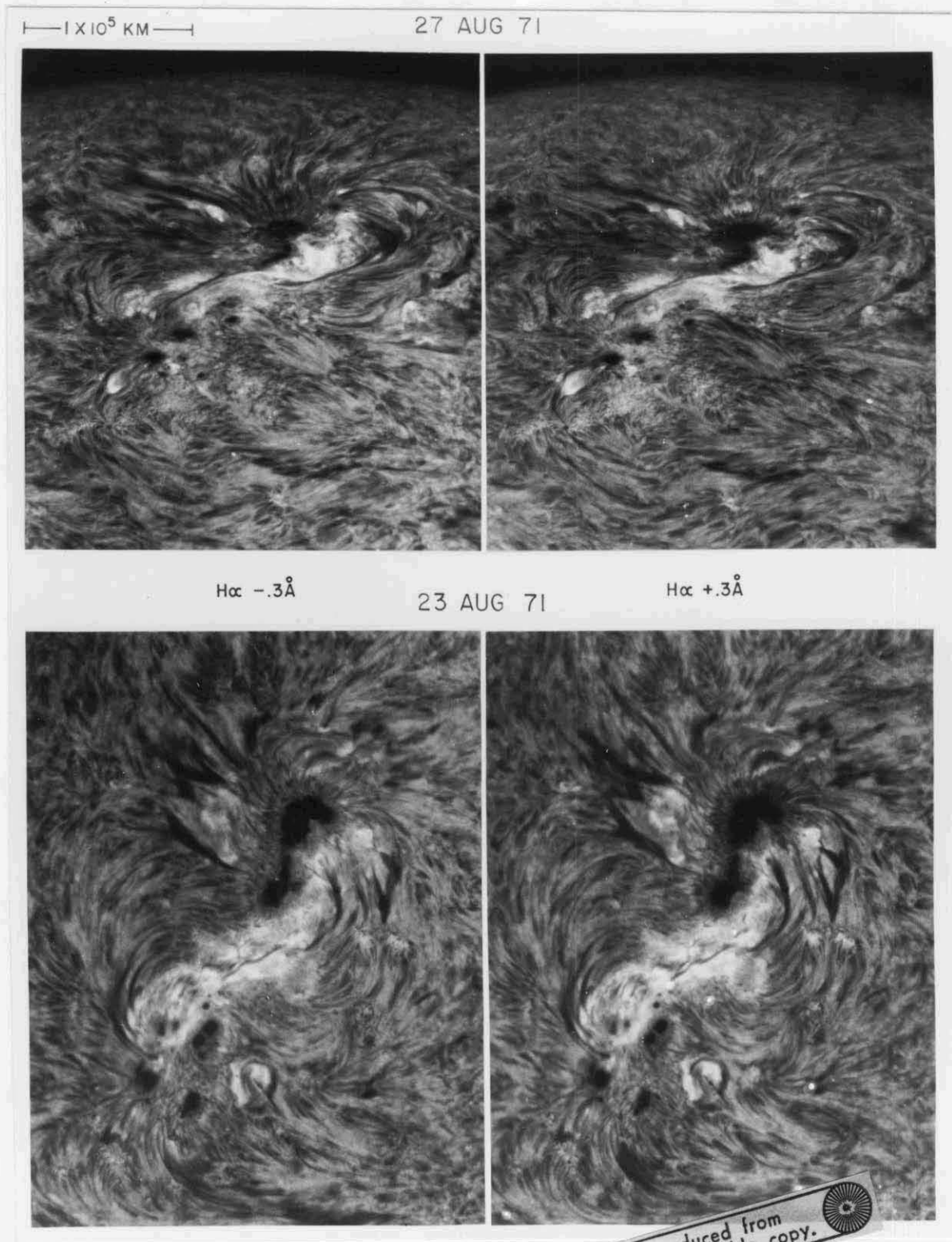


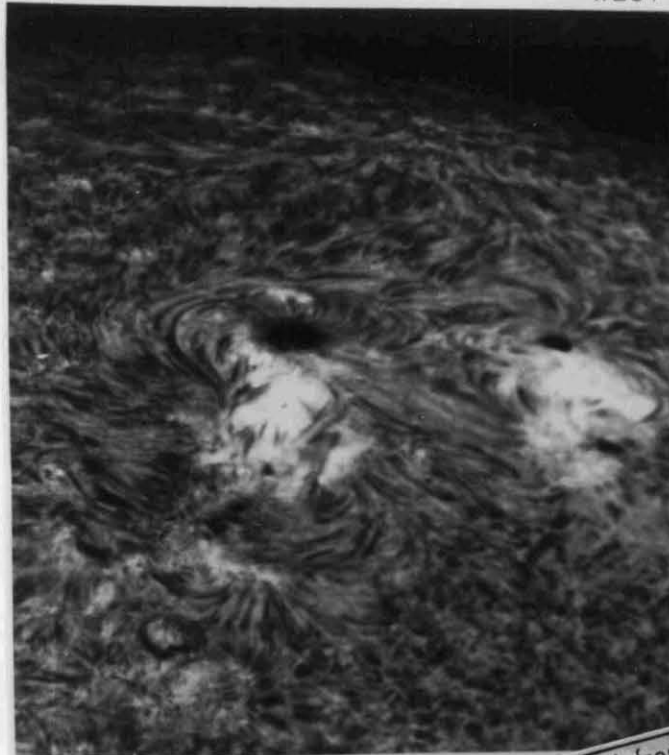
Figure 2.5. Evershed flow into the spot when near the limb is most visible in the blue wing and on the limb side of the spot. At center disk, Doppler differences are reversed. The filament and fibril structures around the spot are darker in the red wing.

7 SEPT 71

IMSC D24368

— 1×10^5 KM —

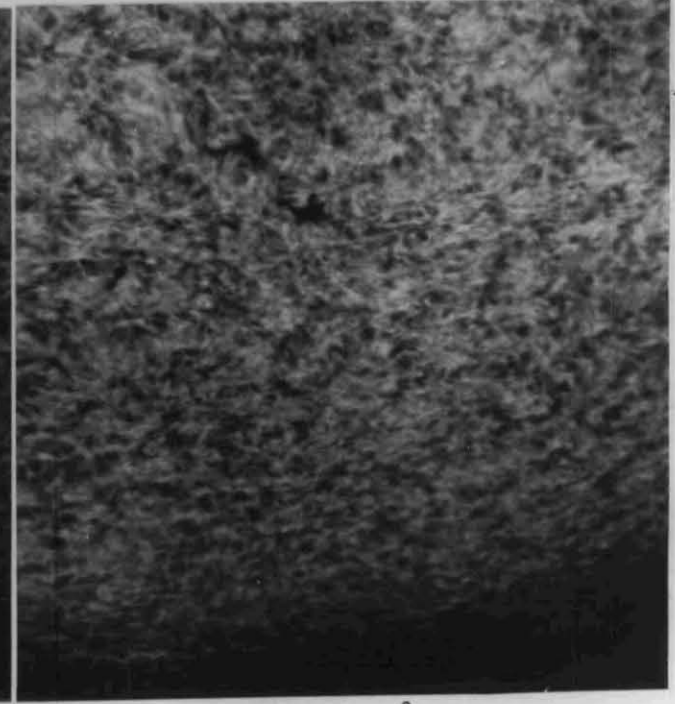
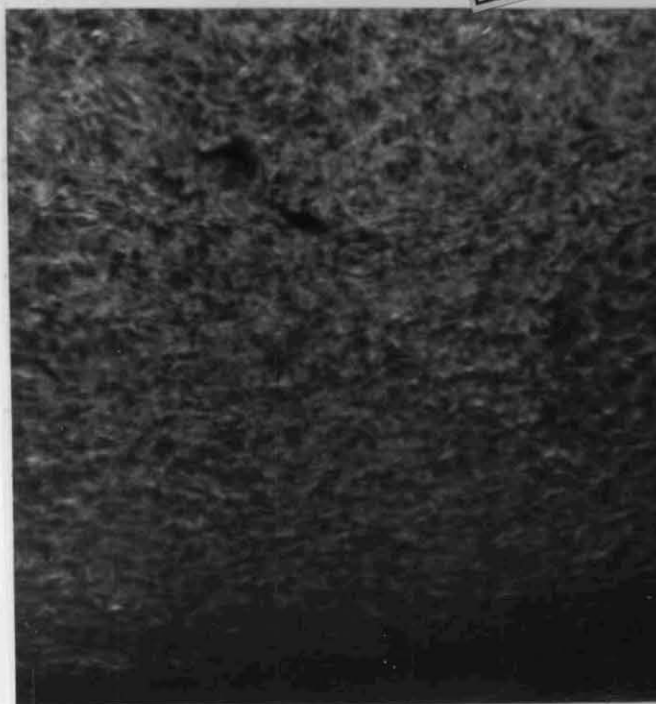
WEST LIMB



$H\alpha - .30 \text{ \AA}$

$H\alpha + .30 \text{ \AA}$

Reproduced from
best available copy.



$H\alpha - .24 \text{ \AA}$

EAST LIMB

$H\alpha + .36 \text{ \AA}$

Figure 2.6. Rotation of the $H\alpha$ chromosphere is seen as a change in background structure dominated by an overall increase or decrease in photospheric light.

Upon changing photographic density to intensity, referencing the film gamma curve, we found a velocity change of 1 km/second is proportional to a 5% change in background intensity. If we couple this observed filter sensitivity with the present sensitivity of video subtraction techniques which can see a 0.1% change in intensity, then we have a potential for observing Doppler velocity changes of 0.05 km/second. This may be a grossly optimistic figure. However, we plan to examine the problem more completely with the possibility of initiating a program of sensitive monitoring of rotation of the H α chromosphere for comparison with the daily Doppler velocity maps prepared by Mt. Wilson Observatory.

REFERENCES

- Bruzek, A. 1967, "Structures and Development of Solar Active Regions (ed. by Kiepenheuer, 293-298, I.A.U.)
- Ellison, M.A. 1949, Monthly Notices Royal Astron. Society 109, 3
- Evershed, J. 1949, The Observatory, 68, 67
- Hyder, C. L. 1967, Solar Physics, 2, 1
- Hyder, C. L., Nakagawa, Y. 1969, Bulletin American Ast. Society, 1, 281
- Weart, S. R. 1970, Astrophys. J. 162, 987-992

SECTION 3

MAGNETIC FEATURES MOVING FROM THE PERIMETER OF SUNSPOTS

3.1 Introduction

Sheeley (1969) discovered on a series of CN spectroheliograms taken over a 2.5 hour period, bright points moving outward from sunspots with velocities of the order of 1 km/sec to distances of about 10,000 km. Vrabc (1971) describes similar features observed on a sequence of Zeeman spectroheliograms (made in the Ca I line, 6102.7 Å). He noted a persistent radial outflow of features of both polarities to where the magnetic network first appears.

More recently, Liu and Sheeley (1971) have identified emission points moving outward from sunspots with velocities of the order of 1 km/sec on a sequence of K_{2v} spectroheliograms taken over a 2.5 hours period at a rate of one per minute. They have interpreted this phenomenon as identical with the bright points observed in CN and with the moving magnetic knots observed by Vrabc.

Because the moving features of magnetic flux appear on K_{2v} spectroheliograms, it is probable that they extend into the chromosphere. Therefore, it is of particular interest to study $H\alpha$ structure in relation to the occurrence of this phenomenon.

3.2 Observations

As part of a continuing program, simultaneous $H\alpha$ and magnetic field observations were made of several active regions from 15-18 October and 28-31 October 1970. At Lockheed Solar Observatory high resolution $H\alpha$ filtergrams were taken using a 1 Å band-pass filter. During these $H\alpha$ observations, magnetograms were made with the best possible spatial resolution using the new 40-channel magnetograph (Livingston and Harvey, 1971) at the Kitt Peak National Observatory. The magnetic field data were then reduced to computer-generated pictures, where the departure from grey is proportional to the square root of the observed magnetic field. An example is shown in Figure 1.

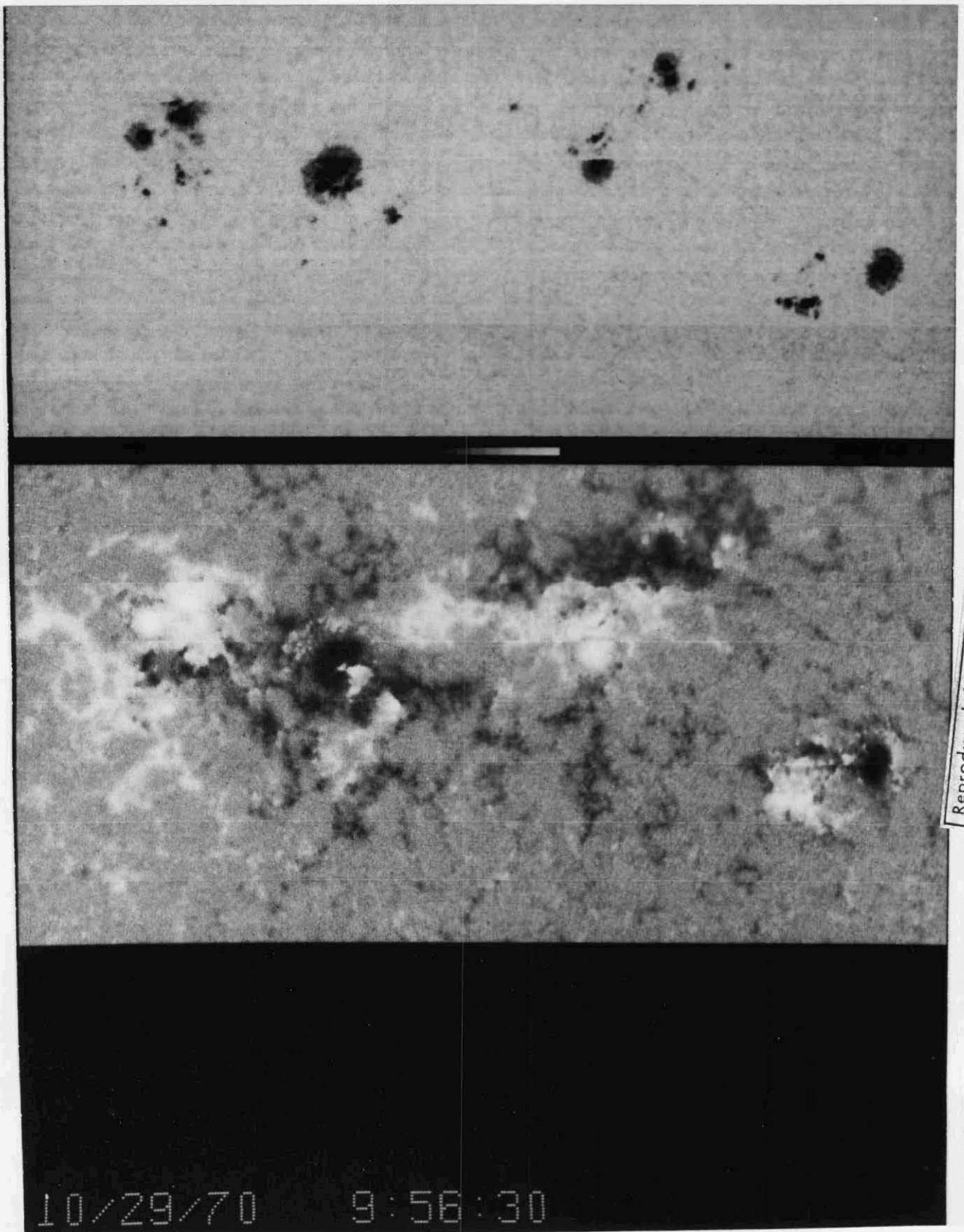


Figure 1. Computer-generated picture of sunspots and corresponding magnetic fields observed on 29 October 1970. Note the numerous dot-like magnetic features surrounding the largest sunspots.

Information concerning the observations is listed in Table I.

3.3 Results

In this section we discuss the characteristics of the moving magnetic features as observed on the magnetograms and their relation to $H\alpha$ structure.

Because of the nature of the display, the most obvious moving magnetic features have a polarity opposite to that observed for the parent spot, as shown in Figure 1. When the sequence of magnetograms is viewed as a movie, moving magnetic features of both polarities are observed, as has been found by Sheeley (1971) and Vrabcic (1971). In general, however, it is difficult to isolate or to follow same polarity features on individual magnetograms. Our results, therefore, pertain specifically to the opposite polarity features.

The sequence of magnetograms in Figure 2 illustrates the appearance and behavior of the moving magnetic features. The magnetic features (dark) first appear near the outer edge of the penumbra and move outward from the parent spot (light) located near the center of the frame. When the features reach the network field, they vanish. No feature has been observed closer than 1500 km to the outer edge of the penumbra.

The features are seen as either single elements or as a collection of small concentrated areas (which may appear at the same time) roughly forming an arc around the sunspot, as in Figures 1 and 2. The individual elements making up the arc do not necessarily move outward with the same velocity.

The moving magnetic features are unresolved even with these high resolution magnetograms. Because they are unresolved, we are unable to accurately establish the field strength or flux, though a lower limit to the flux can be determined.

For the lower resolution magnetograms, the absolute value of the flux ranges from 3.3×10^{17} to 2.5×10^{19} maxwells and for the higher resolution magnetograms from 1.1×10^{17} to 1.4×10^{19} maxwells. If we assume the flux is concentrated into one resolution element, we find the longitudinal field strength ranges from 10 to 750 g for the lower resolution magnetograms

TABIE I

OBSERVATIONS: COOPERATIVE PROGRAM, 15-18 OCTOBER AND 28-31 OCTOBER 1970

DATE 1970	Hr Hours Observed (UT)	Magnetograms Hours Observed (UT)	Time Magnetogram (min)	Area Scanned (arc-min)	Entrance Aperture (arc-sec)
15 October	1612-2312	1555-2316	18	7.5 x 4.2	1.25
16 October	1600-2316	1513-2320	18	7.5 x 4.2	1.25
17 October	1557-1730	1512-1732	18	7.5 x 4.2	1.25
18 October	2001-2330	2004-2330	18	13.3 x 6.7	2.5
18 October	1636-1955	1456-2240	18	13.3 x 6.7	2.5
28 October	1603-2420	2249-2309	20	14.2 x 6.7	2.5
29 October	1605-2412	1504-2222	19	14.2 x 6.7	2.5
29 October		1656	38	14.2 x 6.7	1.25
30 October	1605-2350	1512-2237	38	14.2 x 6.7	1.25
31 October	1605-2400	1538-2224	38	14.2 x 6.7	1.25

Reproduced from
Best available copy.

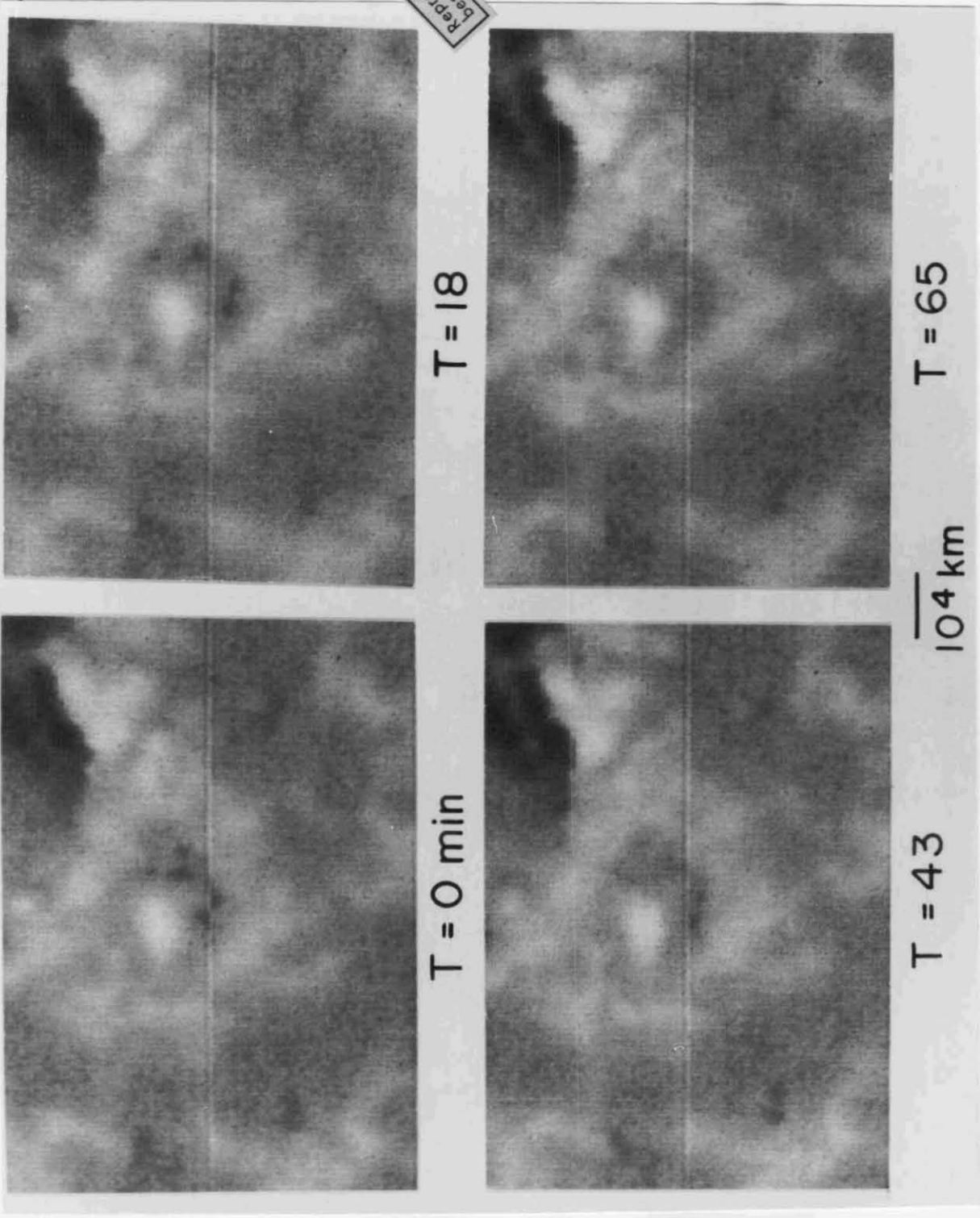


Figure 2. Sequence of magnetograms showing appearance and behavior of the magnetic features moving from the border of a sunspot, 17 October 1970. The 0 minute frame is at 1512 UT. The umbra of the sunspot is the light area in the center of each frame.

(one resolution element is 2.5 arc-sec square) and from 14 to 1800 g for the higher resolution magnetograms (one resolution element is 1.25 arc-sec square).

For five moving magnetic features, we have attempted to eliminate the background fields from the magnetic field measurements of the features by subtracting a magnetogram, where no opposite polarity features were observed, from one with the features. The results are listed in Table II.

TABLE II
COMPARISON OF THE OBSERVED AND CORRECTED
FLUX OF MOVING MAGNETIC FEATURES

Date (1970)	Resolution Element (arc-sec)	Observed Flux (maxwells)	Corrected* Flux (maxwells)
17 October	1.25	-1.2×10^{18}	-3.1×10^{18}
17 October	1.25	-1.3×10^{18}	-3.2×10^{18}
17 October	1.25	-2.3×10^{18}	-4.8×10^{18}
17 October	1.25	-1.1×10^{17}	-2.6×10^{18}
18 October	2.5	-1.9×10^{18}	-1.6×10^{19}

*Flux corrected for background fields

In Figure 3, plots of distance versus time of several of the magnetic features are shown. The velocity of the features during their lifetime appears to be constant within the errors of observation. The velocities of a sample of 54 features ranged from 0.4 to 2.3 km/sec with a mean velocity of 1.1 km/sec. For a few of the features, those having a large flux, the velocity substantially decreases as the feature approaches to within 2000 km of the network as in Figure 4. This effect appears to be due to the longer time (60-90 minutes) for the field of the feature to merge with the network fields than

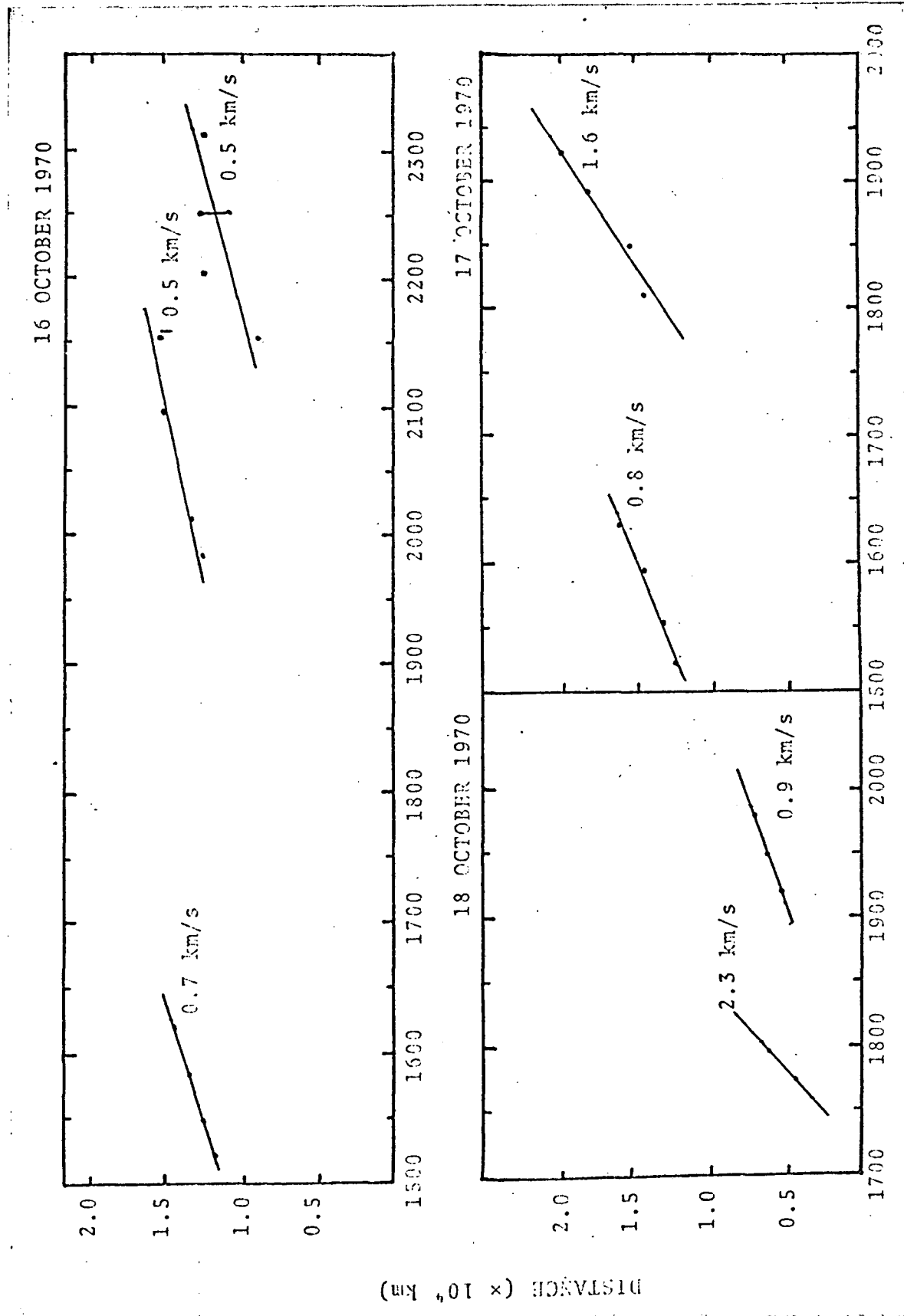


Figure 3. Distance versus time plots of several moving magnetic features. Each plot represents a single path followed by two or more features. The velocities from left to right; 16 October 1970 - 0.7 km/s, 0.5 km/s and 0.5 km/s; 17 October 1970 - 0.8 km/s and 1.6 km/s; 18 October 1970 - 2.3 km/s and 0.9 km/s.

29 OCTOBER 1970

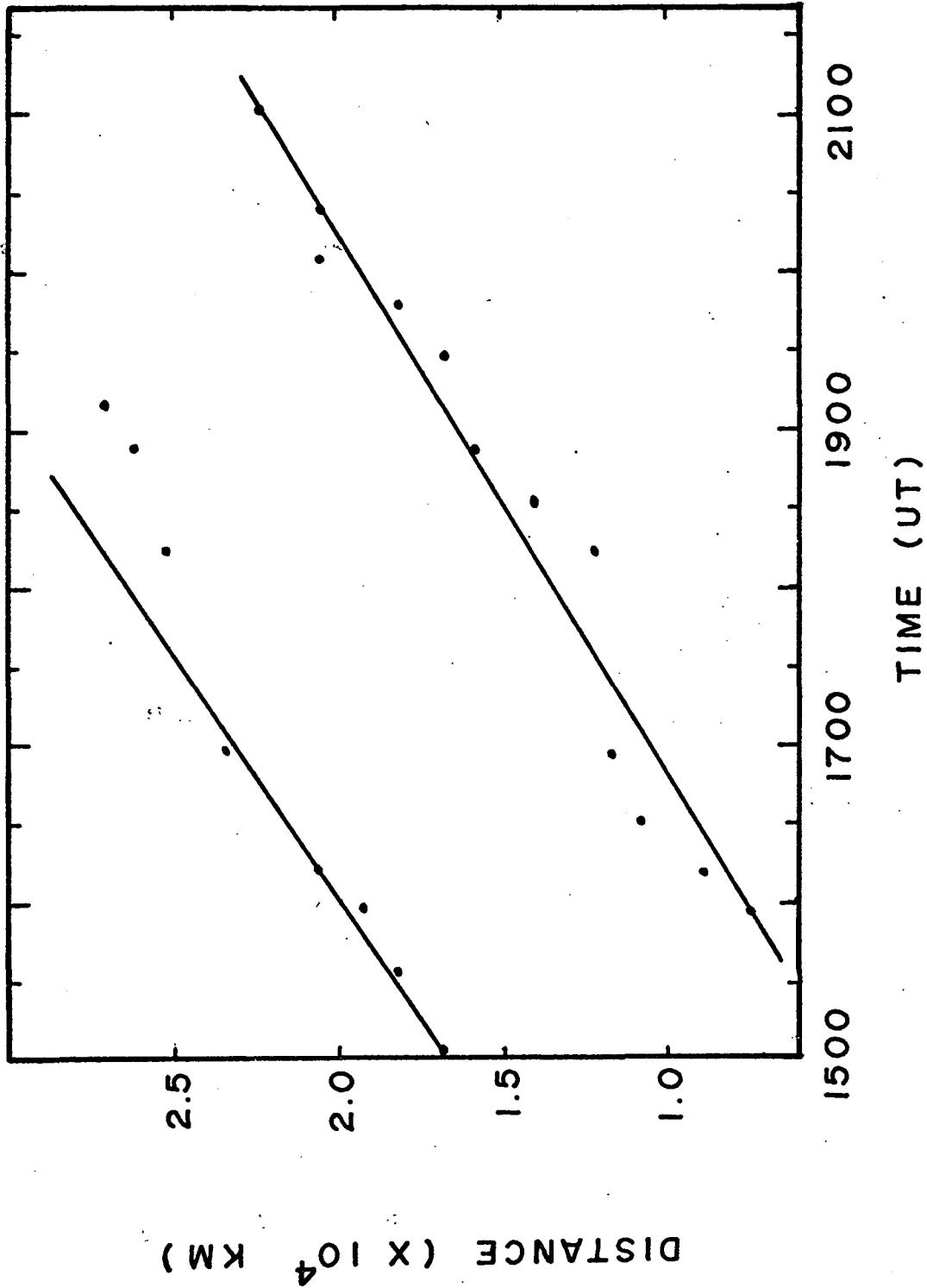


Figure 4. Distance versus time plots of two moving magnetic features following the same path. The velocities from left to right; 0.9 km/s and 0.8 km/s.

we have observed for most of the magnetic features, the merging time being generally less than 30 minutes.

In general, the direction of motion of the magnetic features is approximately radially outward from the parent sunspot. On our observations, more than half of the features followed the same path as previous features. Although they seem to follow the same path, the velocities of successive features can be different, as shown in Figure 3, but in many cases are the same, as shown in Figure 4.

It was of interest to determine if there existed an $H\alpha$ event (flare, surge, etc.) which might mark the initiation, termination, or the passage of the magnetic feature away from the sunspot.

We found no conclusive evidence of any $H\alpha$ feature which might correspond to any aspect of the magnetic feature. In a few cases, an $H\alpha$ event (usually a darkening of a fibril) occurred just prior to and in the vicinity of the magnetic feature. However, similar $H\alpha$ events were observed without any associated magnetic feature.

An examination also was made of high resolution $H\alpha \pm 1.2 \text{ \AA}$ filtergrams at $H\alpha + 1.2 \text{ \AA}$ and $H\alpha - 1.2 \text{ \AA}$ (made with a double 0.2 \AA passband filter) taken from 20 to 30 September 1966 to determine if the bright points observed around sunspots in the wings of $H\alpha$ show any motion similar to that observed for the moving magnetic features. Unfortunately magnetograms of adequate resolution were not available at this time. However, we found no evidence of any motion of the $H\alpha$ bright points. In addition, the lifetimes of the bright points were much shorter than that typically observed for the moving magnetic features observed more recently.

The longitudinal magnetic field configuration of spots associated with the moving magnetic features is exemplified by that shown in Figures 1, 2, and 5. We observe a concentration of field corresponding to the sunspot, a zone of very weak longitudinal field containing the moving magnetic features, and then the network field at about 15,000 km to 25,000 km from the sunspot. Though our sample was small, no moving magnetic features were observed in

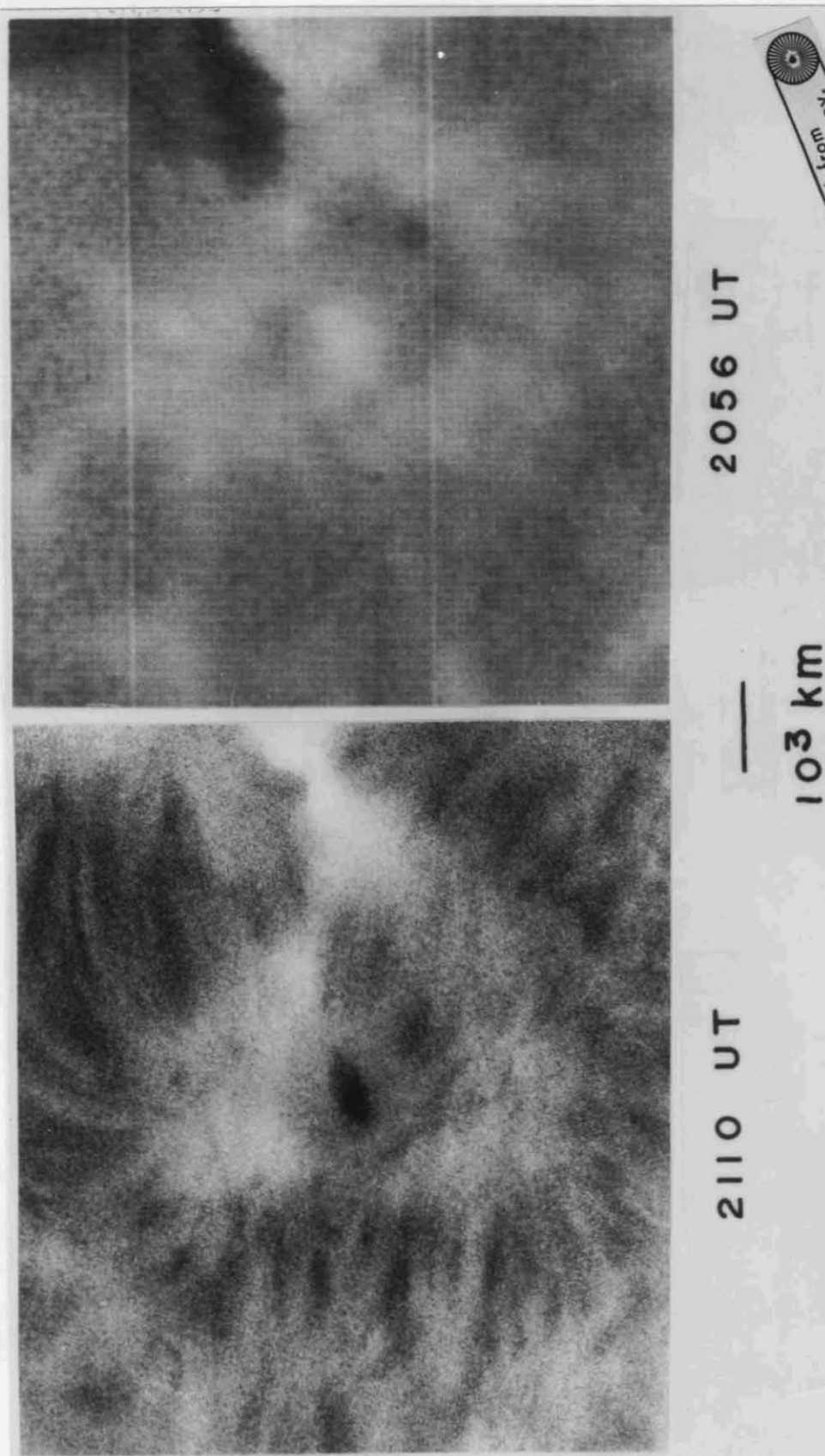


Figure 5. H α filtergram and corresponding longitudinal magnetogram, 16 October 1970.

association with growing spots. Rather, the spots having the moving magnetic features were established or were decaying.

A comparison of H α filtergrams with the magnetograms showed no plage in the weak field zone where the magnetic features were observed. When seeing permitted, we noted H α fibrils in the areas where the magnetic features were observed, as shown in Figure 5. We have observed fibrils in regions where no moving magnetic features are detected; this is not unexpected, since we are undoubtedly seeing only the larger of the magnetic features.

With few exceptions, H α fibrils were aligned with the direction of motion of the magnetic features. Though the lifetimes of the fibrils are 10-20 minutes, the fibril alignment with the direction of motion of the magnetic feature persists during most of the lifetime (1-6 hours) of the magnetic feature. Loughhead (1968) is a study of the fibrils surrounding sunspots (the superpenumbra) found the average lifetime of the fibrils to be 17 minutes though the general orientation of the fibrils did not change over a period of 1.5 hours.

While we do find that the H α fibrils are aligned with the direction of motion of the magnetic features, it is not clear whether or not a direct relation exists between the fibrils and the magnetic features. The lack of plage, the existence of fibrils and the weak longitudinal fields suggest that the moving magnetic features occur where the magnetic field is principally horizontal.

3.4 Discussion

As pointed out previously, Liu and Sheeley (1971) have found evidence of the moving magnetic features extending into the chromosphere. At photospheric levels, we have found that the fields of the moving magnetic features are comparable to that observed for plage fields. However, there does not appear to be a corresponding brightening in H α for the magnetic features as we observe for the plage fields.

Our study has indicated that the H α fibrils surrounding sunspots occur where we observe magnetic features and are aligned with the direction of motion of

the features. In a few instances we have noticed fibrils terminating in or near a magnetic feature. This observation, while not conclusive, suggests that the fibrils connect the sunspot and the moving magnetic features of opposite polarity. One additional observation appears to substantiate the above interpretation. If fibrils follow magnetic field lines as suggested by Loughhead (1968) and Bruzek (1969), then the fibrils must connect areas of opposite polarity. Within the resolution limit of the magnetograms and in most of the regions where the fibrils occur, the only areas of polarity opposite to that of the sunspot are the moving magnetic features.

As the magnetic features move out toward the network fields, conditions along the field lines may change sufficiently to result in the formation of a succession of fibrils, having generally the same orientation.

It is not clear yet how these magnetic features fit into the evolution of active region, but it seems possible that we are seeing a manifestation of the mechanism for the dispersal of sunspot fields suggested by Leighton (1964).

REFERENCES

- Bruzek, A. 1969, Solar Physics 8, 29
- Leighton, R. B. 1964, Astrophys. J. 140, 1547
- Iiu, S. Y. and Sheeley, N.R. 1971, private communication
- Livingston, W. C. and Harvey, J.W. 1971, IAU Symposium No. 43, D. Reidel Publishing Company, Dordrecht, Holland, in press
- Loughhead, R. E. 1968, Solar Physics 5, 489
- Sheeley, N. R. 1969, Solar Physics 9, 347
- Sheeley, N. R. 1971, private communication
- Vrabc, D. 1971, IAU Symposium No. 43, D. Reidel Publishing Company, Dordrecht, Holland, in press

Section 4

HeI D₃ EMISSION FROM FLARE REGIONS

J. L. Kulander

Abstract

The D₃ line intensity in a 1000 km thick plane parallel layer has been calculated assuming the layer to be optically thin. Electron temperatures between 10^4 and 5×10^4 °K and electron densities between 10^{11} and 10^{14} cm⁻³ were considered. The results show that for the D₃ line to appear in emission against the photosphere an electron density of at least about 10^{12} cm⁻³ and an electron temperature of the order of 15,000°K are required.

He D₃ EMISSION FROM FLARE REGIONS

J. L. Kulander

I. INTRODUCTION

The purpose of the theoretical effort this year has been to determine the physical conditions within a flare region which would allow the HeI D₃ line to appear in emission against the photosphere. This emission, as opposed to the usual absorption, has been observed at the Lockheed Rye Canyon facility. The D₃ line represents the transition $3^3D \rightarrow 2^3P^0$ at 5876Å (cf. the energy level diagram in Figure 1). The photospheric radiation at this wavelength is well represented by a blackbody at 6000°K.

Our task then has been to calculate the D₃ line emission from a model flare region and compare it with the photospheric intensity. For the model, we chose a plane-parallel layer with a physical thickness of 1000 km. situated just above the photosphere. A 1000 km layer is a reasonable model based on current observations and understanding of flare phenomena. There are great uncertainties however and this is only an order of magnitude estimate. The temperature range studied was $10^4 - 5 \times 10^4$ °K with the electron density varying from $10^{11} - 10^{14}$ cm⁻³. We assumed that the layer is optically thin in all lines and continua. The results are given in Section IV. We know that such a layer is not in fact optically thin in many resonance lines and continua. The optically thin solution is much less complicated than the thick solutions and represents a logical starting point for the more detailed treatments. The optical thicknesses actually

encountered are discussed in Section V. Unfortunately, time did not permit us to obtain publishable solutions for the optically thick layer during the present study. We did however begin to consider this problem.

A considerable effort was made in obtaining a reliable set of reaction rates for the various bound-bound and bound-free radiative and collisional transitions. Our model HeI atom (Figure 1) contained the 19 energy levels through $n = 4$; the model He II ion (Figure 2) contained nine levels again through $n = 4$. A recent summary of the available cross sections is given by Hearn (1969). We used the results of many of the papers mentioned by Hearn in obtaining our reaction rates. Unfortunately, the rates he obtained and used in his calculations were not presented. The electron impact excitation rates are probably the most uncertain and the most time consuming to tabulate since there are significant transitions between all pairs of levels not just those for which there is an allowed radiative transition. It was noticed that there can be a wide variation in cross sections for electron impact excitation amounting to factors of 10^2 or larger. We decided that it would be very useful if someone were to calculate these rates using all of the available cross sections and to present them in a simple analytical form. This would serve both to illustrate the uncertainties involved in using different cross section results and also eliminate a great deal of time by relieving subsequent investigators of the tedious process of reproducing the published cross sections and numerically integrating them over a Maxwellian distribution. A separate paper has been written discussing these electron-impact excitation rates. The various cross sections and transition probabilities we have used are described in more detail in Section III.

We have not had sufficient time during the present contract to review all of the previous work on the D_3 line emission. We will, however, present in the next section of this final report a summary of some of the more interesting previous studies.

II. PREVIOUS INVESTIGATIONS

The statistically steady state level populations of model HeI atoms have been calculated by a number of investigators for temperatures and densities characteristic of the outer solar atmosphere. Almost none of these authors has considered a sufficiently detailed energy level structure in the model atom to accurately obtain the D_3 line emission. Jefferies (1955) e.g. treats the 2s and 2p levels as a single level. De Jager and de Groot (1957) consider the 2s and 2p terms separately but the term structure of higher levels is ignored. This higher term structure is also ignored by Athay and Johnson (1960). They also neglect the effect of the He II ion processes by using other values for the HeI/He II equilibrium. Athay and Johnson arrive at the conclusion that in the temperature range 40,000-50,000 °K the D_3 line will appear in emission for $n_e \geq 10^{12}$ almost independently of T_e . We shall arrive at a similar conclusion as discussed in section IV.

Zirin (1956) assumes in his calculations that transitions between terms of a given level are of negligible importance in determining the occupation numbers. This is known to be a poor assumption. Shklovsky and Kononovitch (1958) have calculated the D_3 line intensity but have made a number of unrealistic physical assumptions. More recently Hearn (1969) has calculated the occupation numbers of a 4l level HeI atom but he only presents results for the resonance line intensities.

Jefferies (1957) has calculated the D_3 line intensity from a layer assumed to be optically thick in the D_3 line. The transport equation was solved assuming coherent scattering with no photospheric radiation in the line. Jefferies' results are very qualitative since it is known that the D_3 line is probably not optically thick. His results are given in Table I.

Table I

He D₃ Intensity with Respect to Photospheric Continuum

	Te = 10 ⁴	1.25 x 10 ⁴	1.5 x 10 ⁴	2.5 x 10 ⁴
n _e				
10 ¹¹	0.25	0.34	0.39	0.50
10 ¹²	0.99	1.1	1.7	1.9
10 ¹³	2.4	2.8	3.4	4.3
10 ¹⁴	3.6	4.0	5.4	6.3

III. TRANSITION RATES

The atomic processes within HeI and He II used in this calculation are listed below together with references used for the numerical values of the cross sections and rate coefficients.

A. Spontaneous radiative transitions

1. f numbers for all allowed transitions from Wiese, Smith and Glennon (1966)

2. HeI transition $2^3P \rightarrow 1^1S$; Garstang (1967)

3. HeI transition $2^1S \rightarrow 1^1S$; Victor (1967)

4. HeI transition $2^3S \rightarrow 1^1S$; Mathis (1957)

B. Collisional excitation by electron impact

1. HeI: 1^1S to n^3S , n^3P , n^1P , n^1D ; the experimental measurements of St. John, Miller and Lin (1964)

2. HeI: 1^1S to n^3D , n^3F , n^1F ; Ochkur and Brattsev (1965)

3. HeI: Between 2^3S , 2^1S , 2^3P , 2^1P ; Burke, Taylor, Cooper and Ormonde (1967)

4. HeI: 2^3S to n^1S , n^1P , n^1D , n^1F ; Ochkur and Brattsev (1966)

5. He II: 1^2S to 2^2S , 2^2P , 3^2P ; Burke, McVicar and Smith (1964)

6. All optically allowed transitions not specified above; the dipole approximation; Seaton (1962) with cutoff parameter of Saraph (1964)

7. All optically forbidden transitions not specified above; the semi-empirical gaunt factors given by Allen (1963)

C. Photoionization

Photoionization cross sections from all levels are computed using the quantum defect method of Burgess and Seaton (1959).

D. Collisional ionization by electron impact

1. HeI: 1^1S measured values quoted by Kieffer and Dunn (1966)

2. HeI: 2^3S measured values of Long (1967)

3. Collisional ionization rates from all other levels are computed using the semi-empirical formula given by House (1964)

The various inverse rates were calculated from standard equilibrium relationships which are universally valid.

A comparison of the various collisional excitation rates by electron impact is given in a separate paper. The accuracy of the various rates can be inferred from the differences in the rates presented for the same transition using different measured and theoretical cross sections.

IV. HeI - D₃: THEORETICAL LINE INTENSITIES

The level populations of the model HeI and II atoms shown in Figures 1 and 2 have been calculated assuming a statistically steady state. The energy levels, f-numbers, and other parameters are given in our accompanying paper. The method of solution and basic equations have been previously given (Kulander, 1965) for the optically thin situation which we have assumed. The thin atmosphere assumption means that there is no self absorption of radiation emitted by the flare itself and that the external radiation has a constant intensity throughout the flare region. The 1000 km thick flare model has spatially uniform electron temperature and density distributions. This layer is assumed to be irradiated over one hemisphere (which we denote by a dilution factor $w = 0.5$) by a 6000°K blackbody spectrum simulating the solar photospheric radiation.

Figure 3 illustrates the relative concentrations of HeI, HeII and He III for electron densities $n_e = 10^{11}$ and $n_e = 10^{14}$ for $10,000^{\circ}\text{K} \leq T_e \leq 70,000^{\circ}\text{K}$. As $n_e \rightarrow 0$ relative concentrations approach values independent of n_e . The values at $n_e = 10^{14}$ illustrate the departure from this asymptotic value. Figure 4 illustrates the same HeI, II and III equilibrium concentrations only with $w = 0$, i.e. with no external photospheric radiation incident upon the flare model layer. We present this case here and in subsequent figures to show the relative influence of the external photospheric radiation as opposed to the internal particle interactions within the flare. Table II shows the temperatures for which there are equal concentrations of HeI and II, and HeII and III.

TABLE II
TEMPERATURES FOR EQUAL CONCENTRATIONS

	HeI/HeII = 1		HeII/HeIII = 1	
	w = 0.5	w = 0	w = 0.5	w = 0
n_e				
10^{11}	22,100	23,700	67,100	67,100
10^{14}	21,700	22,100	66,200	66,200

The upper level of the D3 line is level 9 and the lower is level 4 on our model. The intensity in the D3 line is given by:

$$I_\nu(\text{D3}) = n_9 A_{94} \bar{\phi}_\nu h\nu_{94} \frac{\Delta x}{4\pi} \quad (1)$$

where n_9 is the population of level 9/cm³, A_{94} is the Einstein transition probability, $\bar{\phi}_\nu$ is the normalized absorption profile, and Δx is the total layer thickness taken to be 10³ km. For a Doppler broadened line profile the line center intensity becomes

$$I_{\nu_0} = \frac{n_9 A_{94} h\nu_{94} \Delta x}{4\pi \sqrt{\pi} \Delta\nu_D} \quad (2)$$

where the Doppler half-width $\Delta\nu_D$ is

$$\Delta\nu_D = \frac{\nu_0}{c} \sqrt{\frac{2kT_e}{M_{\text{He}}}} \quad (3)$$

The intensities obtained from Eq. (2) and divided by the photospheric intensity are shown in Figure 5 for electron densities of 10^{11} , 10^{12} , 10^{13} , and 10^{14} cm^{-3} . The He concentration is assumed to be 10% that of H. The H is assumed to be completely ionized. It is not clear at present how much enhancement of the flare intensity above the background is required to make the flare appear in emission. This is an experimental question which should be further clarified this year. If a 100% increase is necessary then any value above one in Figure 5 will produce emission. It is apparent that a minimum electron density of about 10^{12} cm^{-3} is then required for emission and that unless $n_e > 10^{14}$ cm^{-3} a minimum temperature of 13,000°K is required.

Figure 6 illustrates the effect of the photospheric radiation on the D_3 emission. The ratio of the D_3 line intensity without the photospheric radiation to that with this external radiation is shown. As one would expect the influence of the photospheric radiation is most important when the electron temperature and density are low and therefore excitations by collisions are relatively small. The photospheric excitation can raise the D_3 emission by as much as 50.

V. DISCUSSION

We note that for our model HeI and II atoms there are three resonance lines in both HeI and II. Using the occupation numbers obtained under the thin atmosphere assumption we can estimate the optical thickness in these resonance lines. The subordinate lines are almost always thin because of their small lower level populations. The optical depths so obtained are shown in Figure 7 as a function of T_e for the case $n_e = 10^{11}$, $w = 0.5$. These values would be changed if the populations had been obtained with the resonance lines assumed not optically thin, however the values in Figure 7 represent a first approximation. It is clear from Figure 7 that for temperatures between 13,000 and 40,000°K all three resonance lines in each atom are optically thick and transport equations should be included for each line. We are in the process of improving our model accordingly.

References

- Allen, C. W., "Astrophysical Quantities", The Athlone Press, Univ. of London, 2nd ed., 1963
- Athay, R. G. and Johnson, H. R., Ap. J. 131, 413, 1960
- Burke, P. G., Cooper, J. W., and Ormonde, S., Phys. Rev. Ltr. 17, 345, 1966
- Burke, P. G., Taylor, A. J., Cooper, J. W., and Ormonde, S., "Fifth International Conference on the Physics of Electronic and Atomic Collisions", Leningrad, 1967
- Burgess, A., and Seaton, M. J., M. N. 120, 9, 1960
- Garstang, R. H., Ap. J. 148, 579, 1967
- Hearn, A. C., M. N. 142, 53, 1969
- House, L. L., Astr. Phys. J. Supp. 81, Vol. VIII, 307, 1964
- Jager, C. de and Groot, C. de, B. A. N. 14, 21, 1957
- Jefferies, J. T., Aust. J. Phys. 8, 335, 1955
- Jefferies, J. T., M. N. 117, 493, 1957
- Kieffer, L. J. and Dunn, G. H., Rev. Mod. Phys. 38, 1, 1966
- Kulander, J. L., J. Q. S. R. T. 5, 253, 1965
- Long, D. R., Thesis, Univ. of Wash., Seattle, 1967
- Mathis, J. S., Ap. J. 125, 318, 1957
- Ochkur, V. I. and Brattsev, V. F., Opt. Spectr., USSR 19, 274, 1965
- Ochkur, V. I. and Brattsev, V. F., Soviet Astronomy - AJ 9, 797, 1966
- St. John, R. M., Miller, F. L. and Lin, C. C., Phys. Rev. 134, A888, 1964
- Saraph, H. E. Proc. Phys. Soc. 83, 763, 1964

Seaton, M. J., Proc. Phys. Soc. 79, 1105, 1962

Shklovsky, I. S. and Kononovitch, E. W., Russ. Ast. J. 35, 37, 19

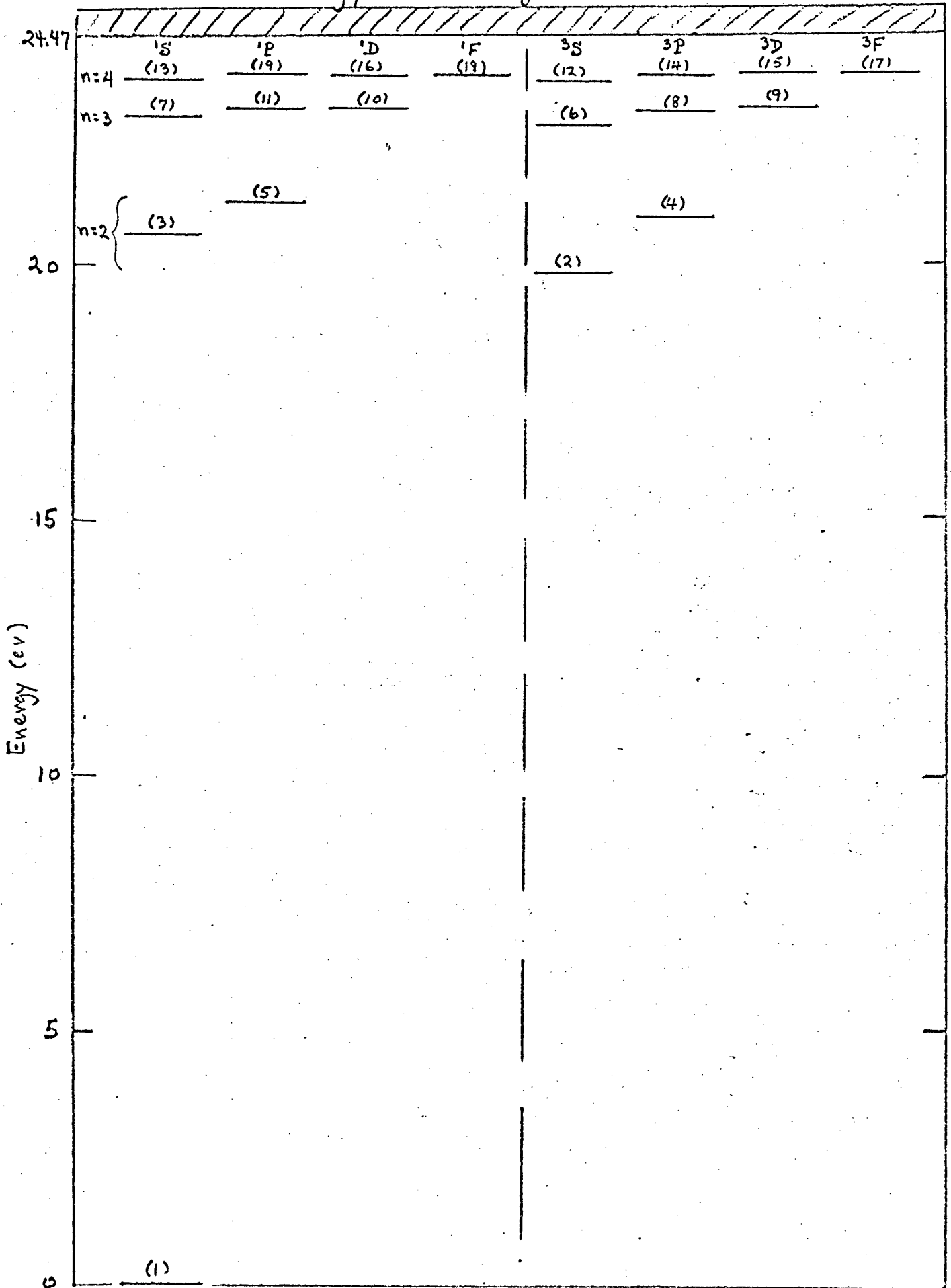
Victor, G. A., Proc. Phys. Soc. 91, 825, 1967

Weise, W. L., Smith, M. W. and Glennon, B. M., "Atomic Transition Probabilities", N SRDS-NBS⁴, Vol. I, 1966

Zirin, H., Ap. J. 123, 536, 1956

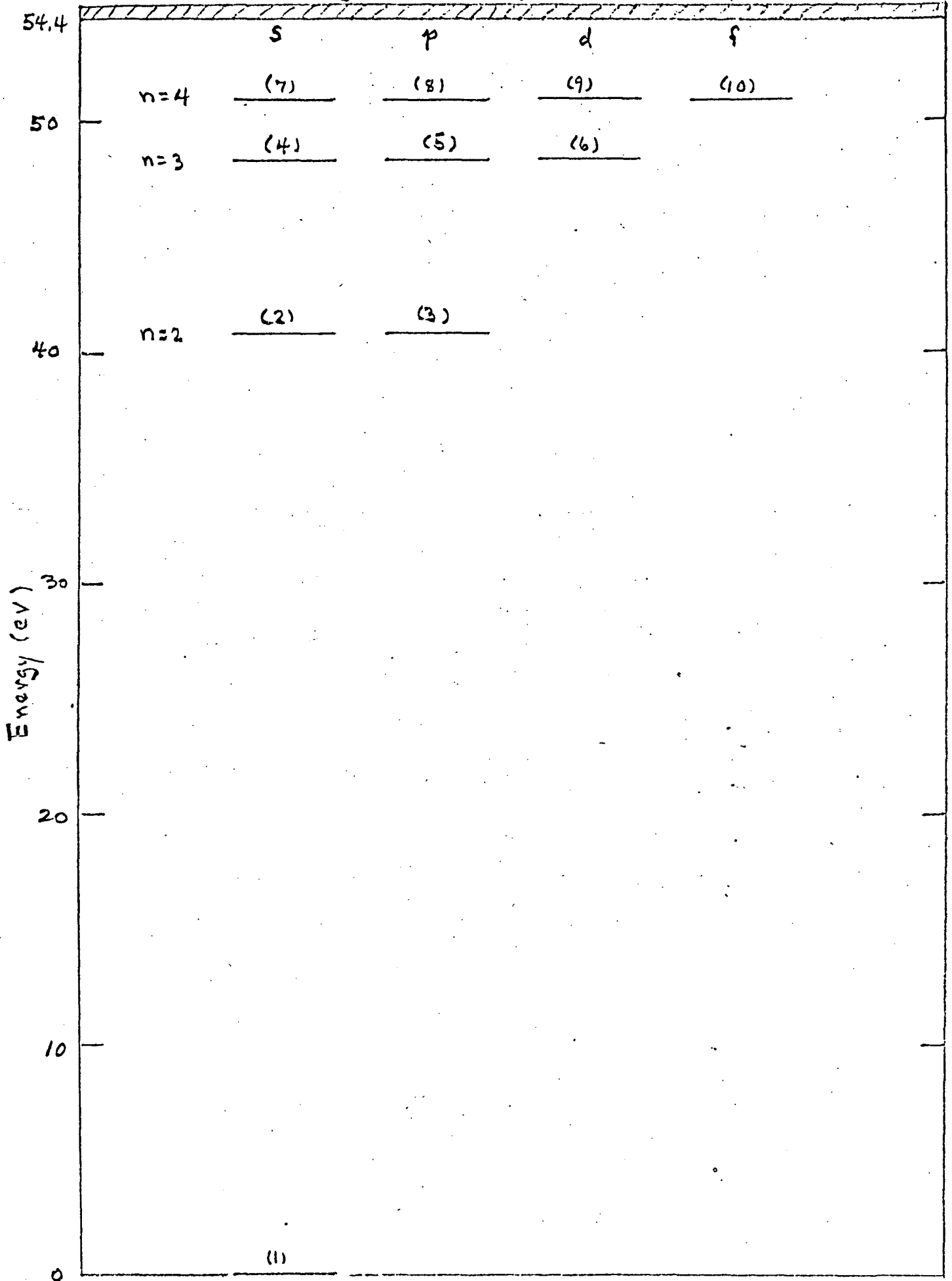
Energy Level Diagram for He I

Fig. 1



Energy Level Diagram for He II

F-16.2



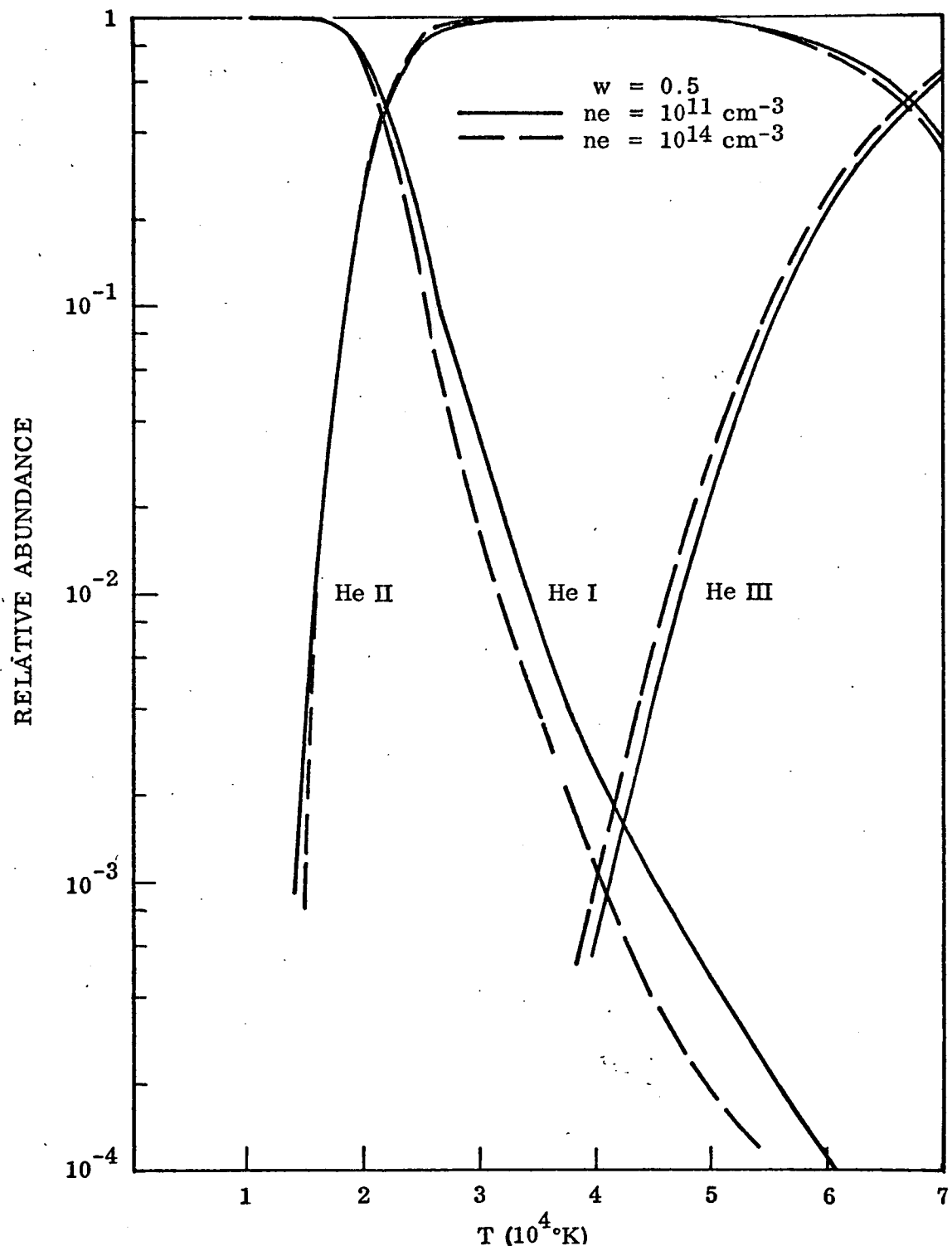


Fig. 3 Ionization Equilibrium — Optically Thin Case

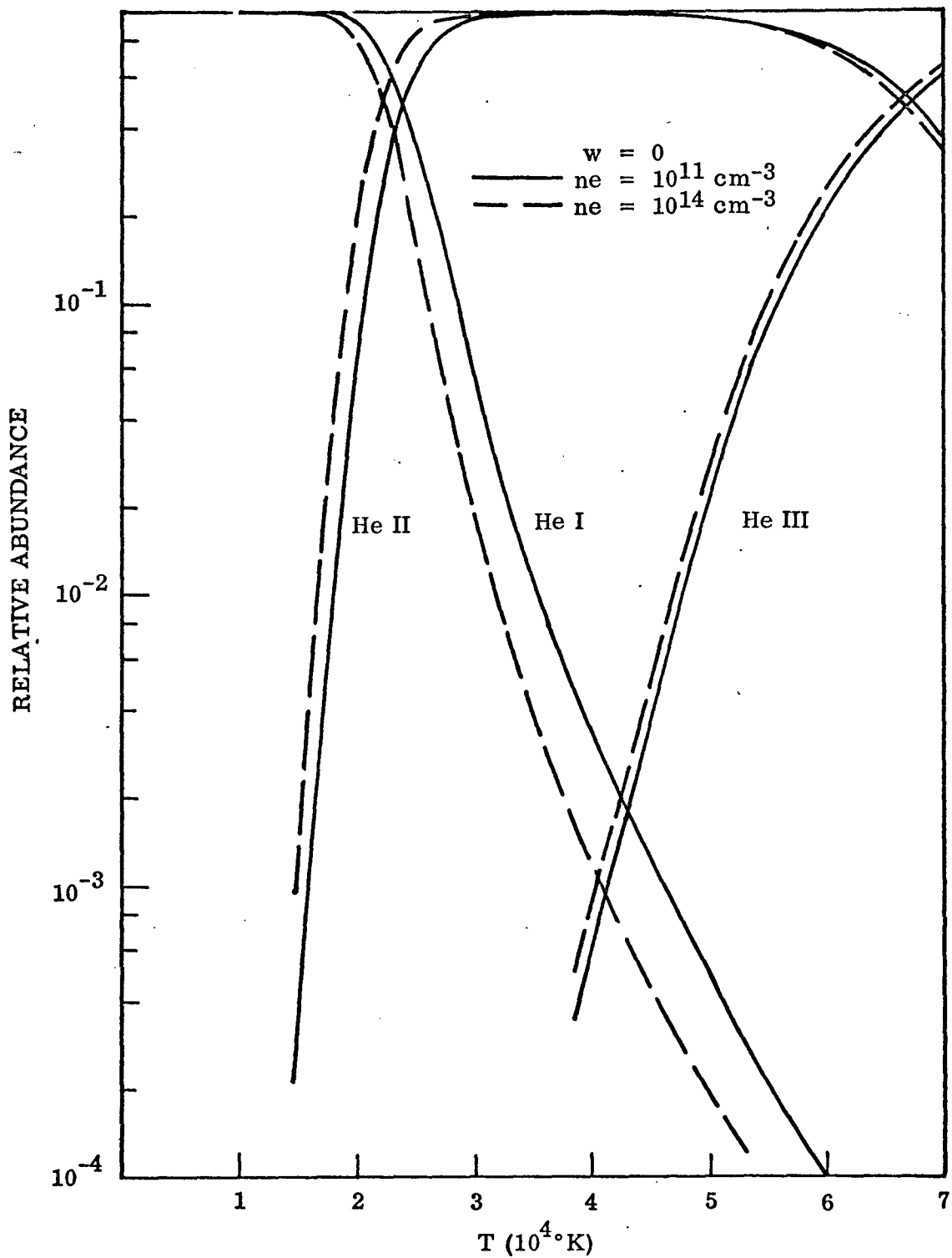


Fig. 4 Ionization Equilibrium - Optically Thin Case

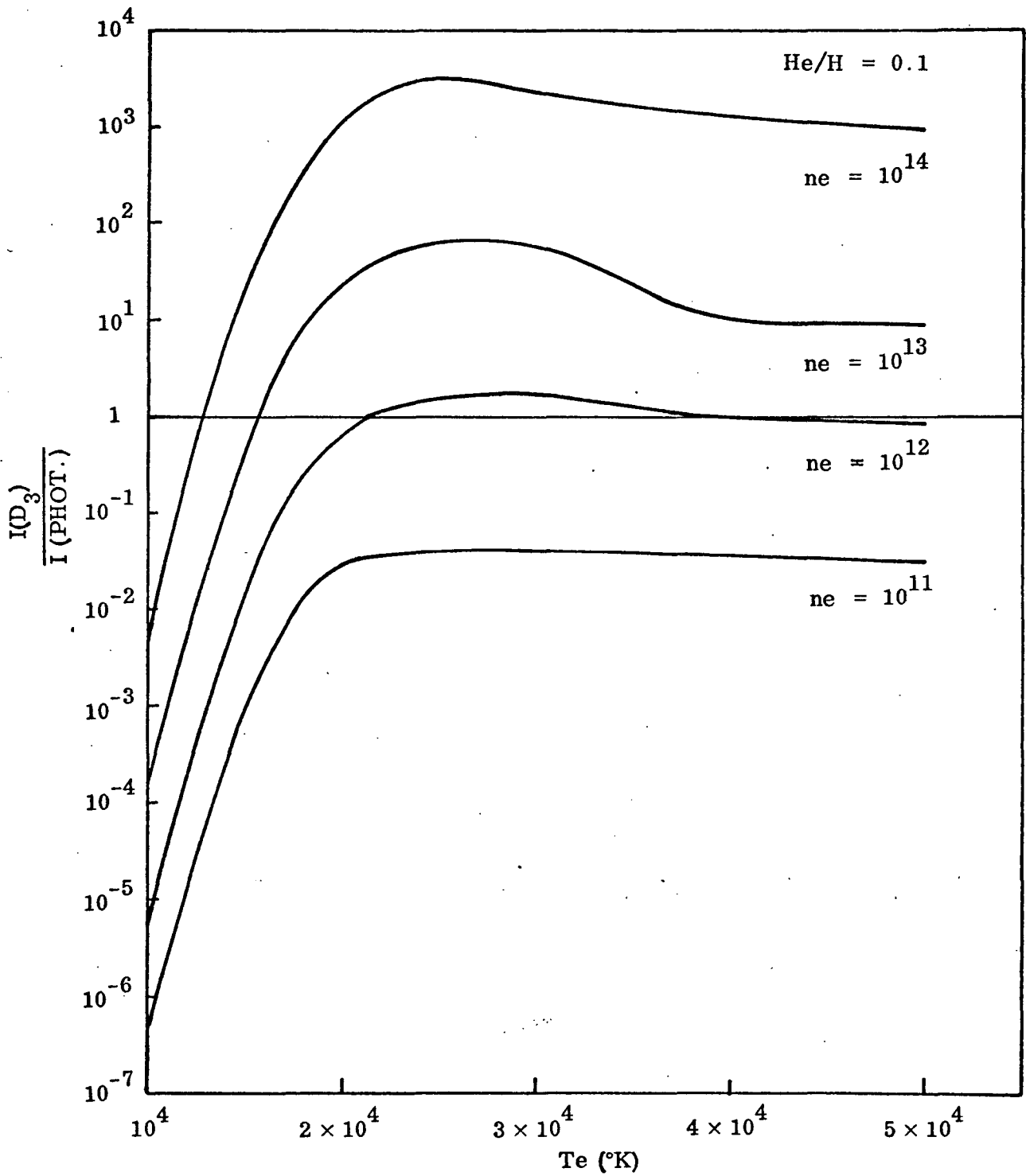


Fig. 5 D3 Line Intensity Relative to Photosphere

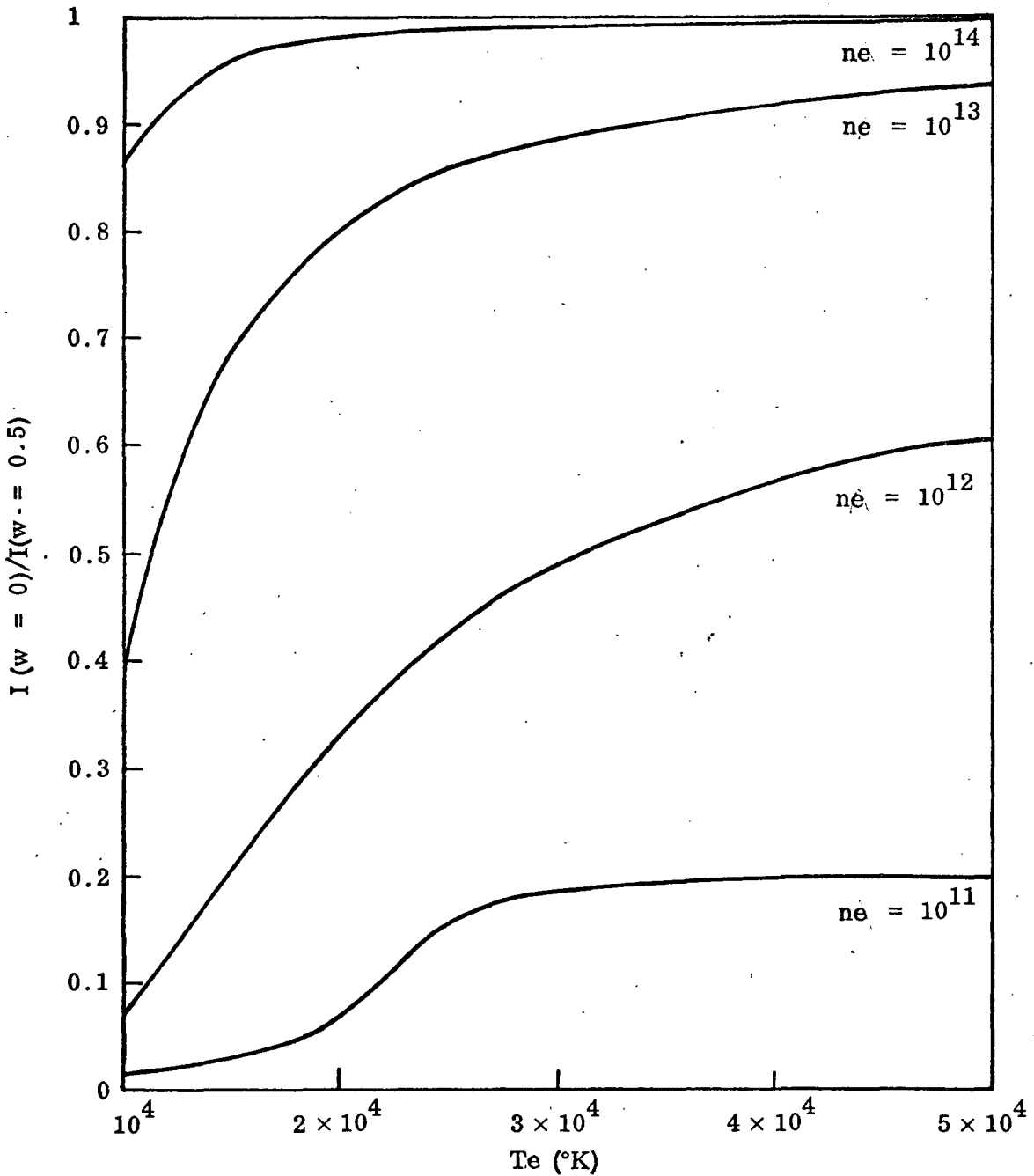


Fig. 6 He D3 Line Intensity With and Without Photospheric Radiation

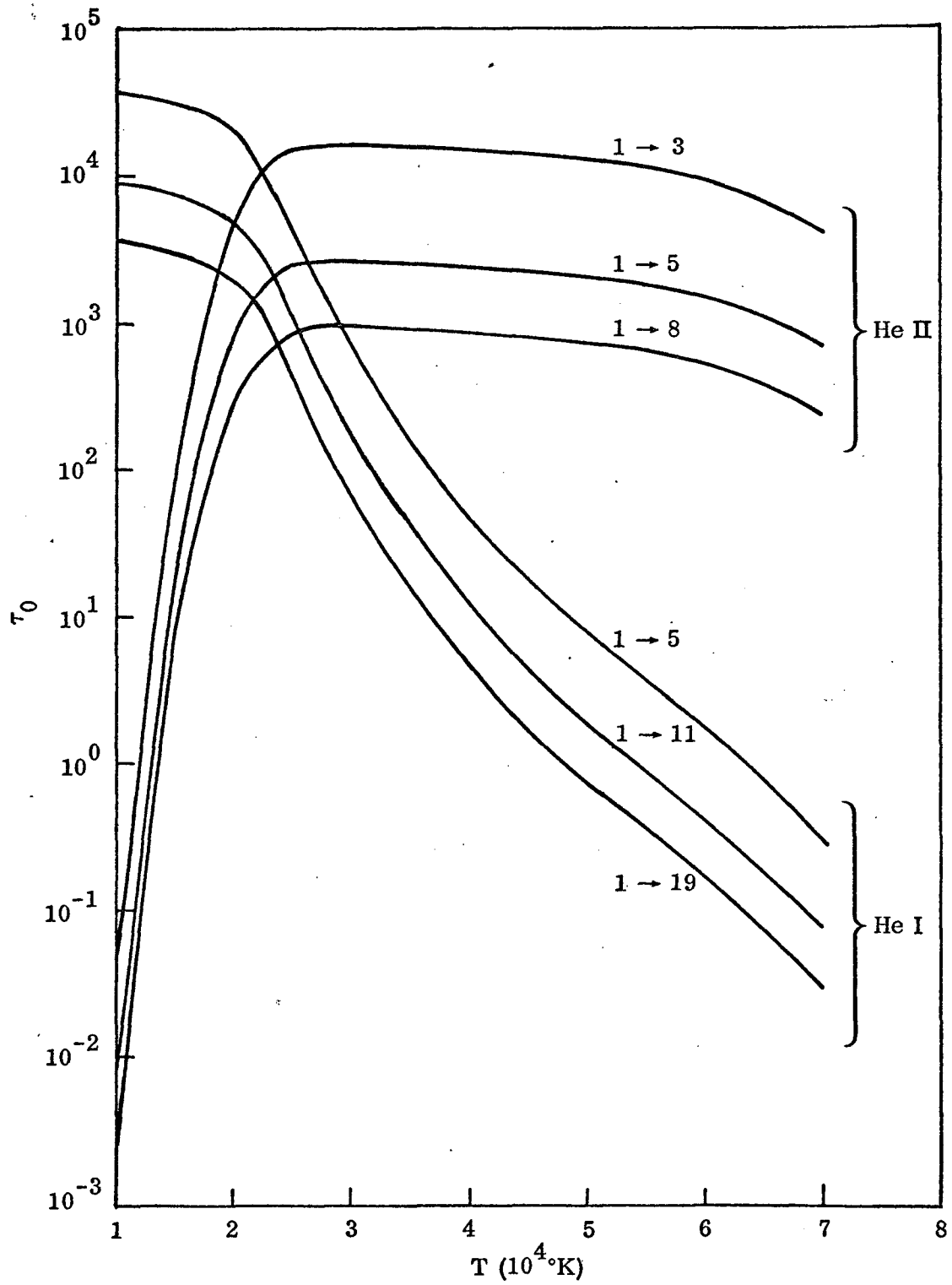


Fig. 7 Optical Depth at Line Center, τ_0